

# Circular Orbits in the Taub-NUT and mass-less Taub-NUT Space-time

Parthapratim Pradhan<sup>1</sup>

*Department of Physics  
Vivekananda Satavarshiki Mahavidyalaya  
(Affiliated to Vidyasagar University)  
West Midnapur, West Bengal 721513, India*

## Abstract

In this work we study the equatorial causal geodesics of the Taub-NUT(TN) space-time in comparison with *mass-less* TN space-time. We emphasized both on the null circular geodesics and time-like circular geodesics. From the effective potential diagram of null and time-like geodesics, we differentiate the geodesics structure between TN spacetime and mass-less TN space-time. It has been shown that there is a key role of the NUT parameter to changes the shape of pattern of the potential well in the NUT spacetime in comparison with mass-less NUT space-time. We compared the ISCO (innermost stable circular orbit), MBCO (marginally bound circular orbit) and CPO (circular photon orbit) of the said space-time with graphically in comparison with mass-less cases. Moreover, we compute the radius of ISCO, MBCO and CPO for *extreme* TN black hole. Interestingly, we show that these *three radii* coincides with the Killing horizon i.e. the null geodesic generators of the horizon. Finally in Appendix-A, we compute the center-of-mass energy for TN BH and mass-less TN BH. We find in both cases the center-of-mass energy is finite. For *extreme* NUT BH, we find the infinite amount of center-of-mass energy. This is *first* we observe that a non-asymptotic extreme spherically symmetric, stationary spacetime showing such feature. In Appendix-B, we compute the *Lyapunov exponent* for null circular geodesics and *quasi normal modes (QNM) frequency* in the *eikonal limit* for both TN BH and mass-less TN BH.

## 1 Introduction

The Taub-NUT (Newman, Unti and Tamburino) space-time [1, 2] is a stationary, spherically symmetric and non-asymptotically flat solution of the vacuum Einstein equation in general theory of relativity. The space-time has topology  $\mathbb{R} \times S^3$  with Lorentzian signature [3]. The NUT space-time is described by two parameters: one is mass  $M$  and another

---

<sup>1</sup>E-mail: pppradhan77@gmail.com

is NUT parameter  $n$ . There is no modification required in the Einstein-Hilbert action to accommodate the NUT charge [4] or “dual mass” [5, 6] or “gravito-magnetic mass” or “gravito-magnetic monopole” [7]. This dual mass is an intrinsic feature of general theory of relativity. The space-time contains closed time-like and null lines. It is geodetically incomplete space-time [3].

't Hooft and Polykov [8, 9] demonstrated that the magnetic monopole present in certain non-Abelian gauge theories. Zee [4] observed that there is an existence of a gravitational analog of Dirac's magnetic monopole [10]. The author is also discussed regarding the mass quantization following the idea of Dirac quantization rule. He also claimed that there is certainly no experimental evidence of mass quantization. Moreover, he proposed that if mass is quantized there may have profound consequences in physics. For example, if a magnetic monopole moving around a nucleus then the mass quantization rule suggests that the binding energy of every level in the nucleus is also quantized. Friedman and Sorkin [11] observed that the gravito-pole may exist in topological solution.

The Euclidean version of the space-time is closely related to the dynamics of BPS (Bogomol'nyi-Prasad-Sommerfield) monopoles [12]. The experimental evidence of this dual mass has not been verified till now. There may be a possibilities of experimental evidences in near future and it was first proposed by Lynden-Bell and Nouri-Zonoz [13] in 1998. Letelier and Vieira [14] have observed the manifestation of chaos for test particles moving in a TN space-time perturbed by dipolar halo using Poincare sections. Geodesics structure in Euclidean TN space-time has been studied in the Ref. [15].

The gravito-magnetic lensing effect in NUT space-time was first studied by Nouri-Zonoz et al. [16] in 1997. They proved that all the geodesics in NUT spacetime confined to a cone with the opening angle  $\delta$  defined by

$$\sin\delta = \frac{2n}{D\sqrt{1 + \frac{4n^2}{D^2}}} \quad (1)$$

where  $D = \frac{L}{E}$  is the impact factor. For small  $\alpha$  and in the limit  $\frac{2n}{D} \ll 1$ , it should be

$$\alpha \cong \frac{2n}{D} \quad (2)$$

It should be noted that the opening angle is proportional to the NUT parameter  $n$ .

They also examined the lensing of light rays passing through the NUT deflector. This properties modified the observed shape, size and orientation of a source. It has been also studied there that there is an extra shear due to the presence of the gravito-magnetic monopole, which changes the shape of the source. The same author also studied electromagnetic waves in NUT space through the solutions of the Maxwell equations via newman-penrose null tetrad formalism to further deeper insight of the physical aspects of the dual mass. Since the Taub-NUT (TN) space-time has gravito-magnetic monopole that changes the structure of the accretion disk and might offer novel observational prospects [17, 18].

The maximal analytic extension or Kruskal like extension of the TN space-time shows that it has some unusual properties [19]. Maximal analytic extension is needed in order to understand the global properties of the space-time. Misner and Taub have shown that TN space is maximally analytic i.e. it has no Hausdorff extension [3]. Whereas Hajicek [20] showed that the non-Hausdorff property occurs only on the Killing horizons and causes no geodesics to bifurcate.

Chakraborty and Majumdar [21] have derived the exact Lense-Thirring precession (inertial frame dragging effect) in case of TN space-time in comparison with mass-less TN space-time. The *mass-less dual mass* (i.e. TN space-time with  $M = 0$ ) concept was first introduced by Ramaswamy and Sen [5]. They also proved that ‘in the absence of gravitational radiation magnetic mass requires either that the metric be singular on a two dimensional world sheet or the space-time contain closed time-like lines, violating causality’. After that Ashtekar and Sen [22] demonstrated that the consequences of magnetic mass in quantum gravity. They also proved dual mass implies the existence ‘wire singularities’ in certain potentials for Weyl curvature. Finally, Mueller and Perry [23] showed the ‘mass quantization’ rule regarding the NUT space-time.

In [24], the author has been studied  $SU(2)$  time-dependent tensorial perturbations of Lorentzian TN space-time and proved that Lorentzian TN space-time is unstable. Geodesics of accelerated circular orbits on the equatorial plane has been studied in detail of the NUT space using Frenet-Serret procedure[25].

However, in the present work we wish to investigate the complete geodesic structure in TN space in the equatorial plane. We compare the circular geodesics in the TN space-time with mass-less TN space-time and zero NUT parameter by *analyzing the effective potential graphically for both null cases and time-like cases*. The presence of the dual mass could changes the geodesic structure in comparison with mass-less dual mass and zero dual mass. This is clearly manifested in the effective potential diagram. We also differentiate *graphically* the ISCO, MBCO and CPO of the said space-time in comparison with mass-less cases. Moreover, we examine the circular geodesics in the  $L - r$  plane for different values of energy i.e.  $E^2 > 1$ ,  $E^2 < 1$  and  $E^2 = 1$  in case of TN and mass-less TN spacetime, and plotted graphically. Furthermore, we have studied more exotic cases i.e. extreme cases, where we find surprising results that the radii of three important class of orbits namely, the radius of ISCO ( $r_{isco}$ ), the radius of MBCO ( $r_{mbco}$ ) and the the radius of CPO ( $r_{cpo}$ ) are coincident with the horizon. From the best of my knowledge, this is first obseved in this work for any spherically symmetric, stationary and *non-asymptotically* flat spacetime. Finally, we shortly compute the center-of-mass energy for this spacetime and we show that for non-extreme spacetime the the center-of-mass energy is finite and for *extreme* NUT spacetime the center-of-mass energy is infinite.

The circular geodesics studied earlier by several authors [18, 7] but they have not been studied in more graphically. We here show differences between two spacetime with mass parameter and mass-less parameter in visually. It may be noted that circular orbits of arbitrary radii are not possible, there exists a minimum radius below which no circular

orbits are possible. The geodesic structure has been studied earlier for Schwarzschild BH [26], Reissner Nordström (RN) BH [26], Kerr-Taub-NUT (KTN) BH [18] and Kerr-Newman-Taub-NUT (KNTN) more recently [27]. In this work, we specialized on the cases when the parameter  $a = Q = 0$ . By studying the geodesic structure we can extract more information about the back ground space-time. Different observables like Lense-Thirring effect, gravitational time delay, gravitational bending of light etc. all are phenomenon related to the geodesics so this is the motivation behind to study them.

The structure of the manuscript is as follows. In section 2, we discuss the basics of TN BH. In section 3, we study the equatorial geodesic properties of the said BH. Section 4 devoted to study the extreme TN BH. The conclusions are given in section 5.

## 2 The TN Space-time:

The metric is given by [1, 19, 28, 29]

$$ds^2 = -\mathcal{H}(r) (dt + 2n \cos \theta d\phi)^2 + \frac{dr^2}{\mathcal{H}(r)} + (r^2 + n^2) (d\theta^2 + \sin^2 \theta d\phi^2) . \quad (3)$$

$$\mathcal{H}(r) = 1 - \frac{2(Mr + n^2)}{r^2 + n^2} \quad (4)$$

where,  $M$  denotes the gravito-electric mass or ADM mass and  $n$  denotes the gravito-magnetic mass or dual mass or magnetic mass of the space-time. It is clearly evident that there are two types of singularity is present in the metric (3). One is at  $\mathcal{H}(r) = 0$  which give us the Killing horizons or BH horizons:

$$r_{\pm} = M \pm \sqrt{M^2 + n^2} \text{ and } r_+ > r_- . \quad (5)$$

$r_+$  is called event horizon and  $r_-$  is called Cauchy horizon.

From Fig.1, we can see the horizon structure of TN and mass-less TN BH. There is a qualitative difference between two horizon structure with NUT parameter and without NUT parameter. In the limit  $n = 0$ , one obtains the Schwarzschild BH. Interestingly, when  $M = 0$ , we get mass-less TN space-time and the horizons at

$$r_{\pm} = \pm n \text{ and } r_+ > r_- . \quad (6)$$

The other type of singularity occurs at  $\theta = 0$  and  $\theta = \pi$ , where the determinant of the metric component vanishes. Misner[28] first demonstrated that in order to remove the apparent singularities at  $\theta = 0$  and  $\theta = \pi$ ,  $t$  must be identified modulo  $8\pi n$ . Provided that  $r^2 + n^2 \neq 2(Mr + n^2)$ . It should be noticed here that the NUT parameter actually measures deviation from the asymptotic flatness at infinity which may be manifested in the off-diagonal components of the metric and this is happening due to presence of the Dirac-Misner type of singularity.

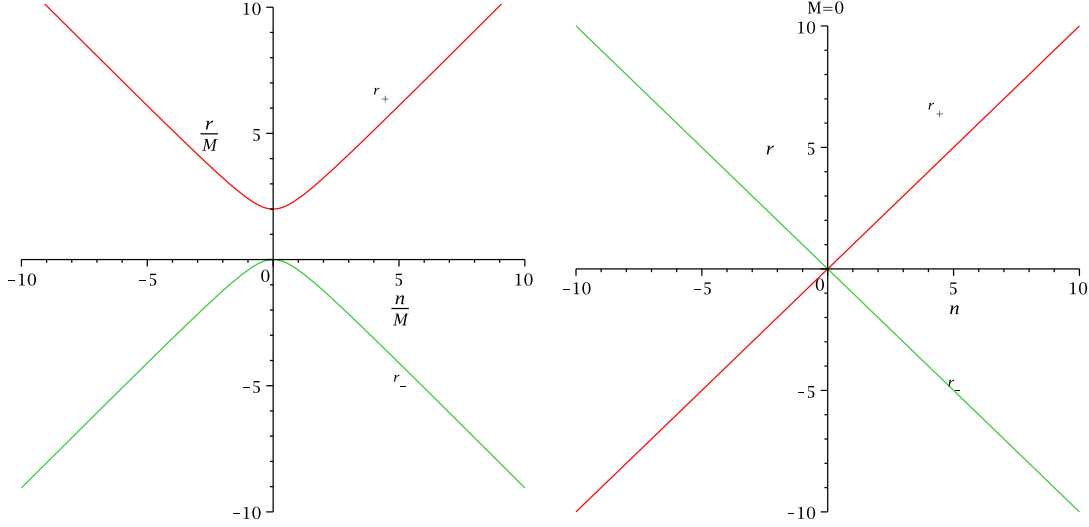


Figure 1: The figure depicts the horizon structure of TN and mass-less TN black hole.

When,

$$M^2 + n^2 \geq 0 . \quad (7)$$

the TN metric describes a BH, otherwise it has a naked singularity. When  $M^2 + n^2 = 0$ , we find extreme TN BH.

The characteristics of the variation of  $-g_{tt}$  with radial coordinate is shown in Fig.2. The “red-shift factor” ( $\mathcal{R}$ ) [30] for TN BH is

$$\mathcal{R} = \frac{d\tau}{dt} = \frac{1}{u^t} = \sqrt{\frac{r^2 - 2Mr - n^2}{r^2 + n^2}} . \quad (8)$$

and for mass-less TN BH is

$$\mathcal{R}_{ml} = \sqrt{\frac{r^2 - n^2}{r^2 + n^2}} . \quad (9)$$

The variation of redshift factor with radial coordinate is shown in Fig.3.

The “red-shift” ( $\mathbf{z}$ ) [30] is given by

$$\mathbf{z} \equiv \frac{\Delta\lambda}{\lambda} = \frac{\lambda_{received} - \lambda_{emitted}}{\lambda_{emitted}} = u^t - 1 = \sqrt{\frac{r^2 + n^2}{r^2 - 2Mr - n^2}} - 1 . \quad (10)$$

For mass-less TN BH it is

$$\mathbf{z}_{ml} \equiv \sqrt{\frac{r^2 + n^2}{r^2 - n^2}} - 1 . \quad (11)$$

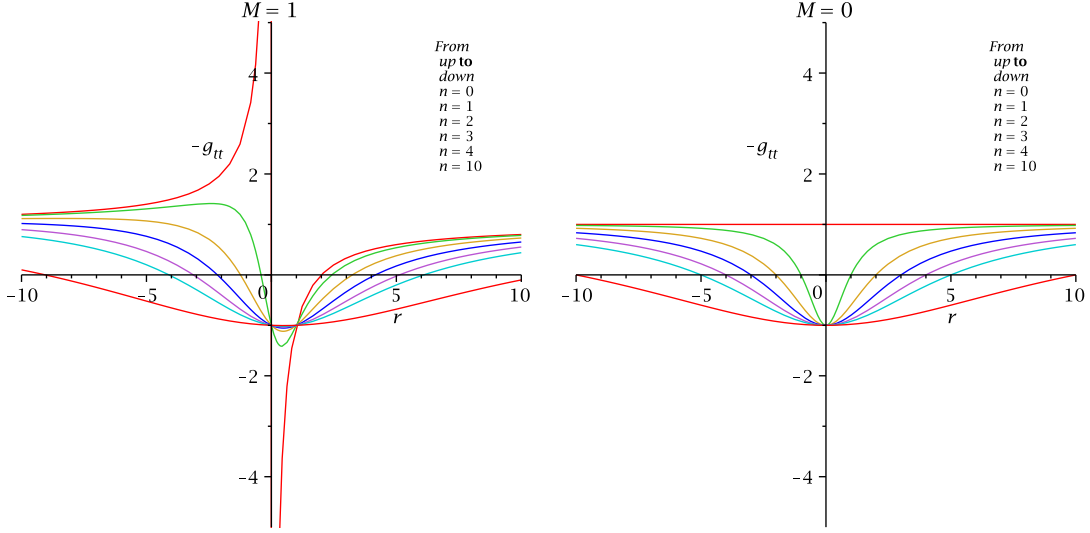


Figure 2: The figure shows the variation of  $-g_{tt}$  with  $r$  for TN and massless TN BH.

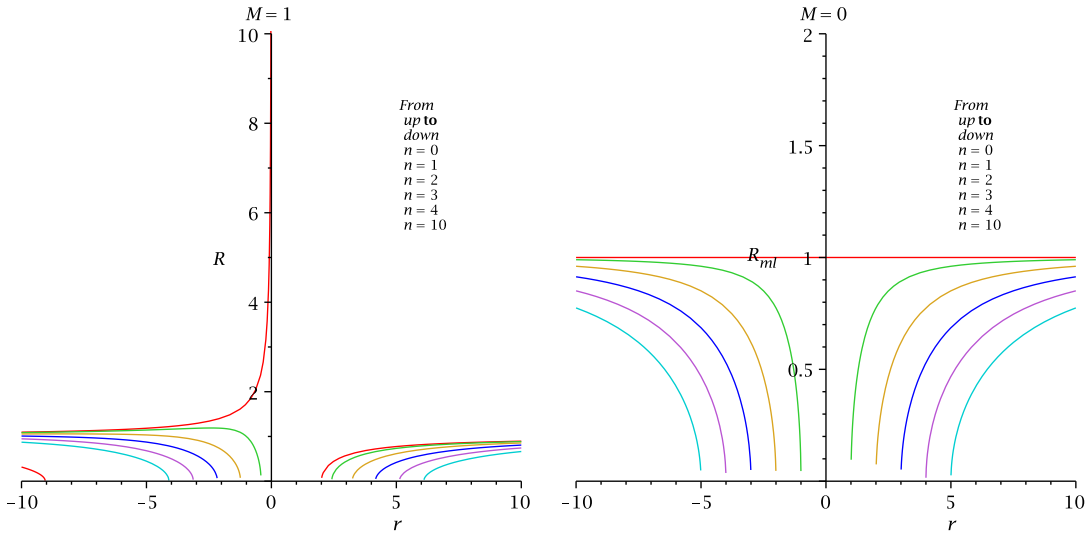


Figure 3: The figure shows the variation of red-shift factor with  $r$  for TN and massless TN BH.

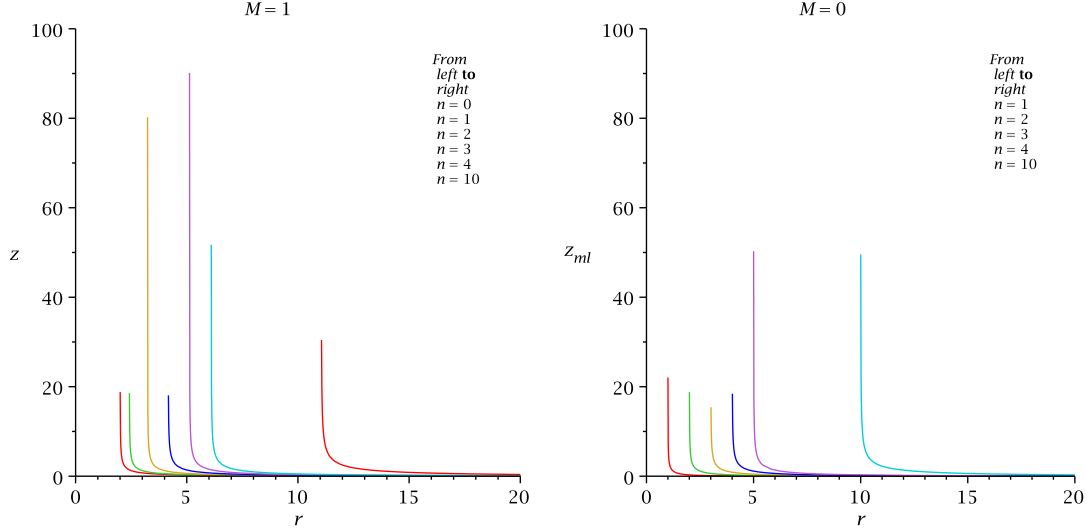


Figure 4: The figure shows the variation of red-shift with  $r$  for TN and massless TN BH.

The variation of redshift with radial coordinate is depicted in Fig.4.

The thermodynamic properties of TN BH could be found in detail in [31] and the BH temperature of  $\mathcal{H}^\pm$  was calculated there

$$T_\pm = \frac{r_\pm - r_\mp}{8\pi (\mathcal{M}r_\pm + n^2)} \text{ and } T_+ > T_- . \quad (12)$$

In the limit  $r_+ = r_-$ ,  $T_+ = T_- = 0$ , this indicates there must exist *extreme* TN BH. The geodesic properties have been studied in Sec. 4.

### 3 Equatorial circular geodesics of the TN BH:

Since the equatorial plane is the good location where we can see the causal characteristics of the geodesics so in this section we would like to study them. It should be noted that  $r = r_0$ , a constant is called circular geodesics. Also, the study of geodesics in the TN space-time is governed by the laws of conservation of energy and angular momentum because the space-time is independent of the coordinates  $t$  and  $\phi$ . The TN space-time possesses time-like isometry generated by the time-like Killing vector  $\xi \equiv \partial_t$  whose projection along the four velocity  $\mathbf{u}$  of geodesics:  $\xi \cdot \mathbf{u} = -E$ , is conserved along such geodesics and the another conserved quantity is angular momentum followed by the relation  $L \equiv \zeta \cdot \mathbf{u}$  (where  $\zeta \equiv \partial_\phi$ ). Where  $\zeta$  is the space-like Killing vector field due to the rotational isometry.

Using these conditions together with the normalization of the four velocity, one can

easily derived the radial equation for TN BH on the  $\theta = \frac{\pi}{2}$  plane:

$$\dot{r}^2 = E^2 - V_{eff} = E^2 - \mathcal{H}(r) \left( \frac{L^2}{r^2 + n^2} - \epsilon \right) . \quad (13)$$

where the effective potential [3] is

$$V_{eff} = \mathcal{H}(r) \left( \frac{L^2}{r^2 + n^2} - \epsilon \right) . \quad (14)$$

Here,  $\epsilon = -1$  for time-like geodesics,  $\epsilon = 0$  for light-like geodesics and  $\epsilon = +1$  for space-like geodesics.

### 3.1 Lightrays orbit:

For light rays orbit, the effective potential becomes

$$U_{eff} = \frac{L^2}{r^2 + n^2} \left( \frac{r^2 - 2Mr - n^2}{r^2 + n^2} \right) . \quad (15)$$

First we see the behaviour of the test particle in the potential well diagram. In Fig 5, Fig 6, Fig 7, Fig 8, Fig 9, Fig 10, Fig 11 and Fig 12, we show how the effective potential for photon changes for different values of angular momentum and NUT parameter. From the effective potential diagram, it has been observed that the presence of *dual mass* effectively changes the shape of the potential well in comparison with absence of *dual mass*. The structure of the potential well also changes in the presence of ADM mass parameter and in the absence of ADM mass parameter.

Now by introducing the impact parameter  $D = \frac{L}{E}$ , one can reparametrization of any null geodesics described by the parameter  $L$  and  $E$ .  $D$  be the angular momentum of null geodesics when it is reparametrized to have unit energy. Now the plot of  $D$  with  $r$  gives the information of radial motion of null geodesics.

The equations evaluating the radius  $r_c$  of the unstable circular photon orbit at  $E = E_c$  and  $L = L_c$  by introducing the impact parameter  $D_c = \frac{L_c}{E_c}$  are

$$r_c^2 + n^2 + \left( \frac{2Mr_c + n^2 - r_c^2}{(r_c^2 + n^2)^2} \right) D_c^2 = 0 . \quad (16)$$

$$r_c - \left[ \frac{Mr_c^2 - Mn^2 + 2n^2r_c}{(r_c^2 + n^2)^2} \right] D_c^2 = 0 . \quad (17)$$

From Eq. (17), we find

$$D_c = \pm \sqrt{\frac{r_c(r_c^2 + n^2)^2}{Mr_c^2 + 2n^2r_c - Mn^2}} . \quad (18)$$



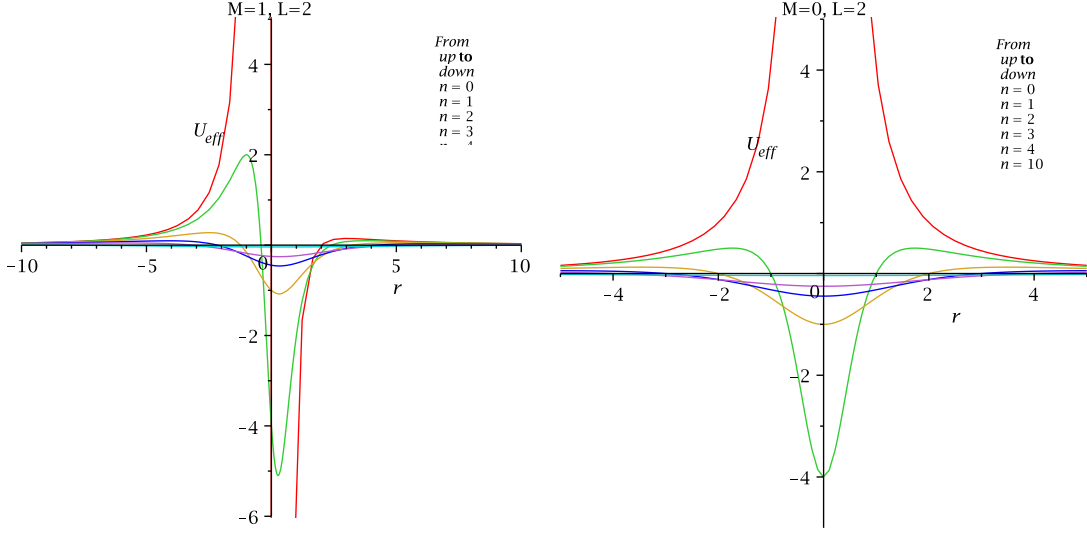


Figure 5: The figure shows the variation of  $U_{eff}$  with  $r$  for TN BH and mass-less TN BH.

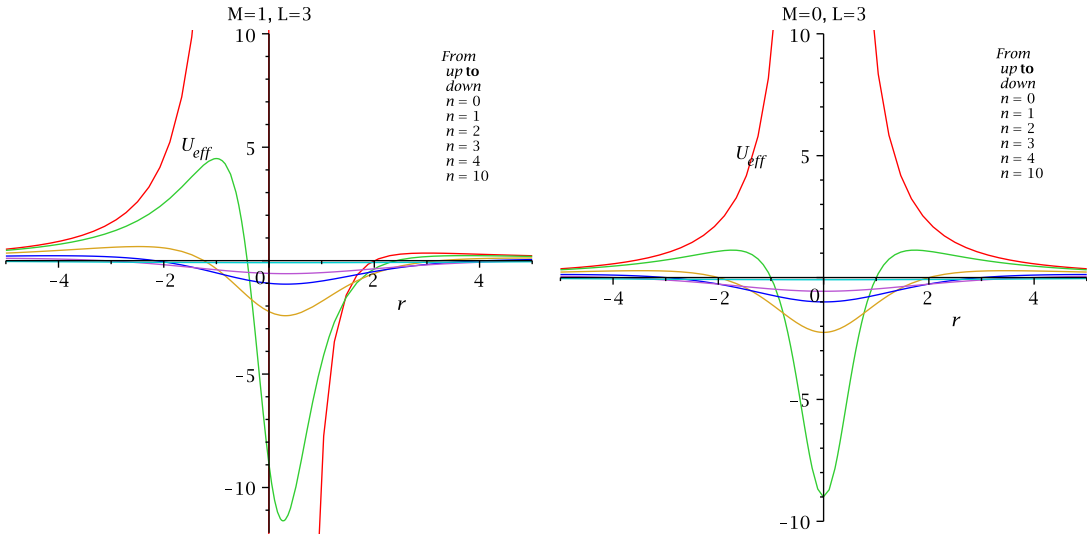


Figure 6: The figure shows the variation of  $U_{eff}$  with  $r$  for TN BH and mass-less TN BH for different values of  $n$ .

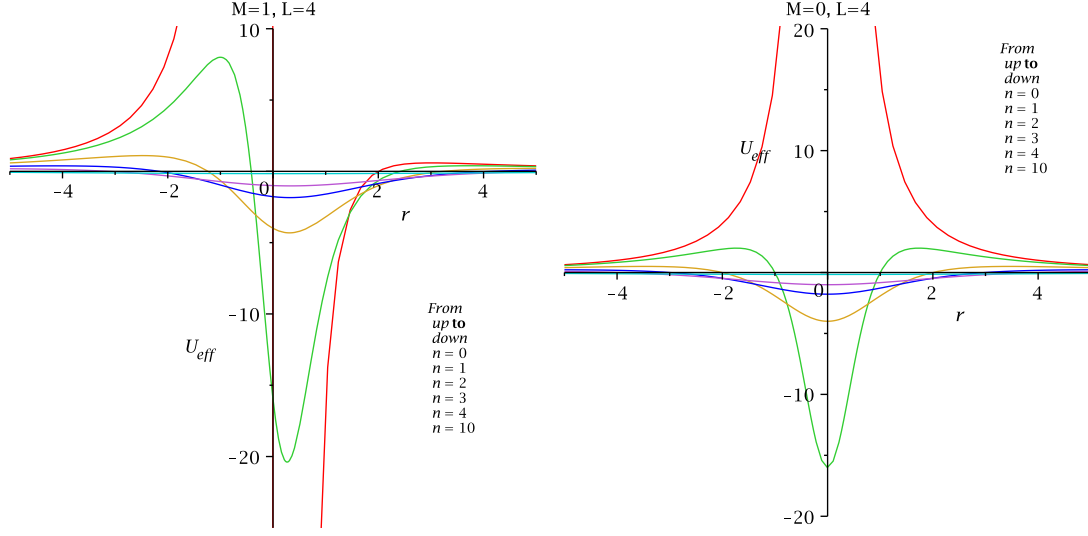


Figure 7: The figure shows the variation of  $U_{eff}$  with  $r$  for TN BH and mass-less TN BH.

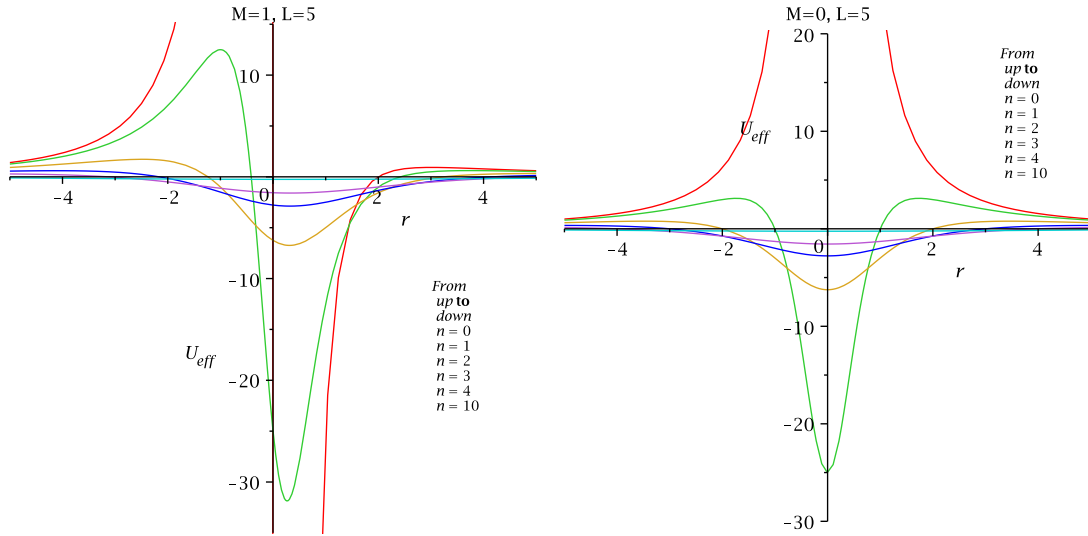


Figure 8: The figure shows the variation of  $U_{eff}$  with  $r$  for TN BH and mass-less TN BH.

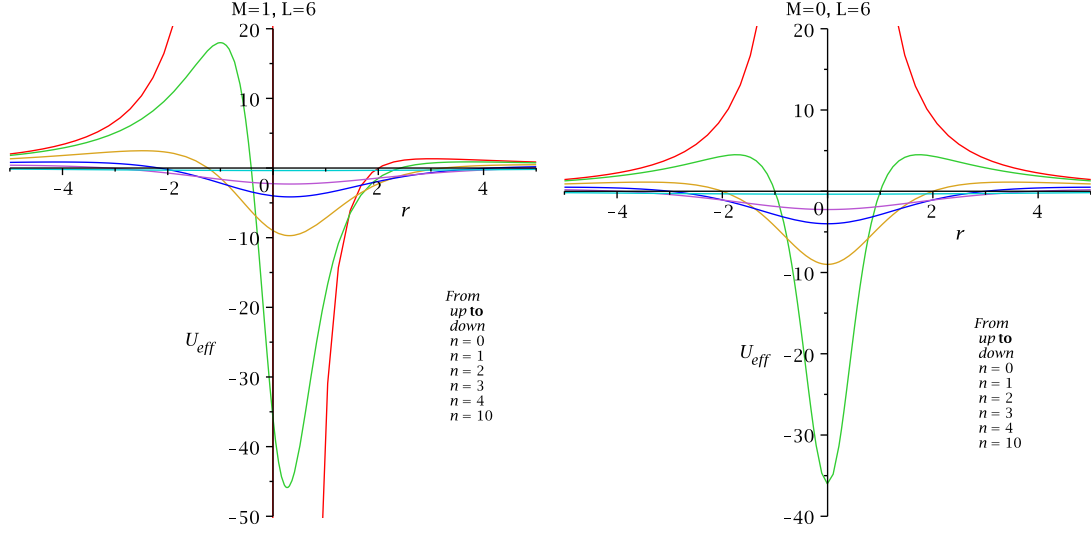


Figure 9: The figure shows the variation of  $U_{eff}$  with  $r$  for TN BH and mass-less TN BH.

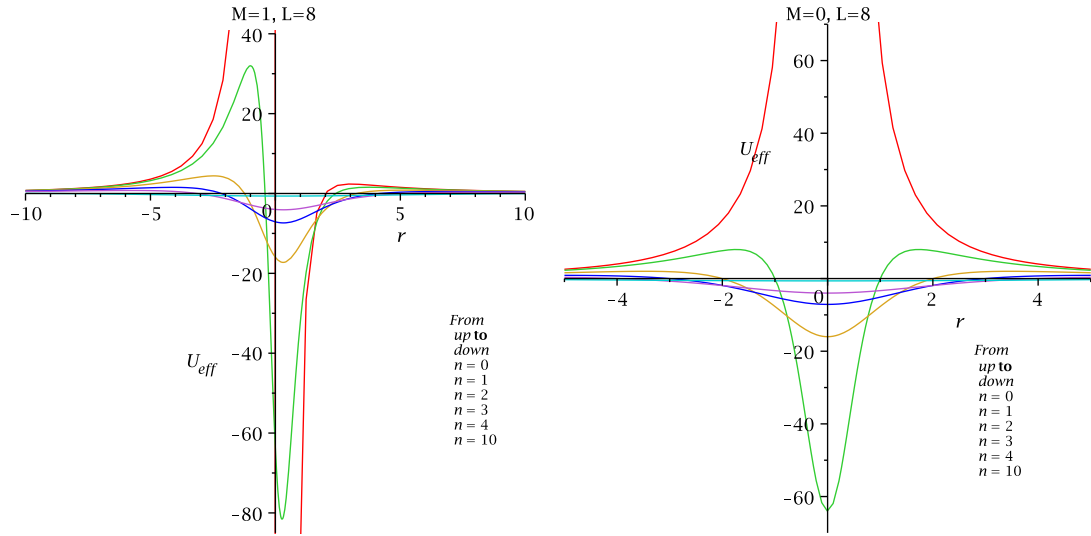


Figure 10: The figure shows the variation of  $U_{eff}$  with  $r$  for TN BH and mass-less TN BH.

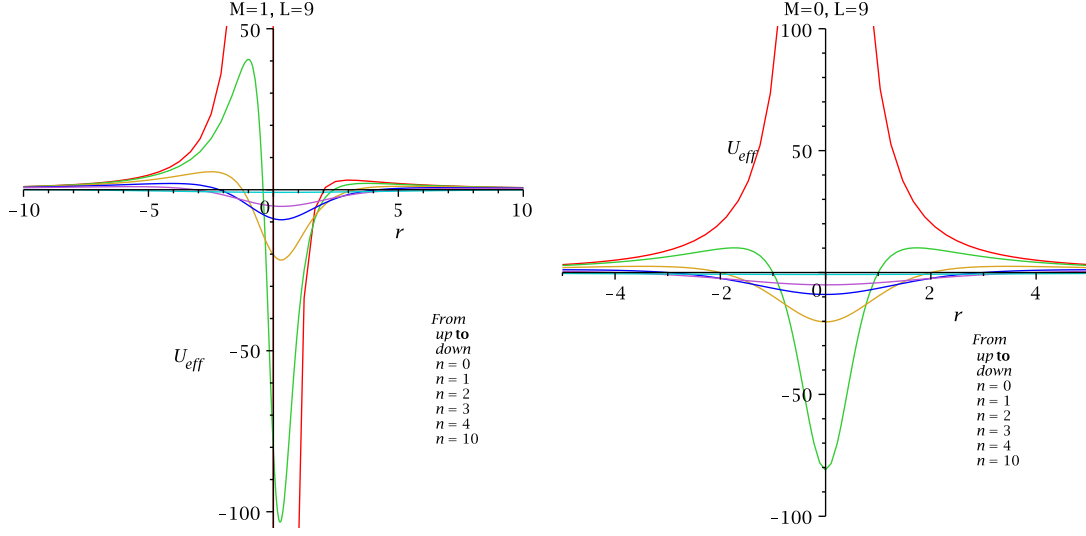


Figure 11: The figure shows the variation of  $U_{eff}$  with  $r$  for TN BH and mass-less TN BH

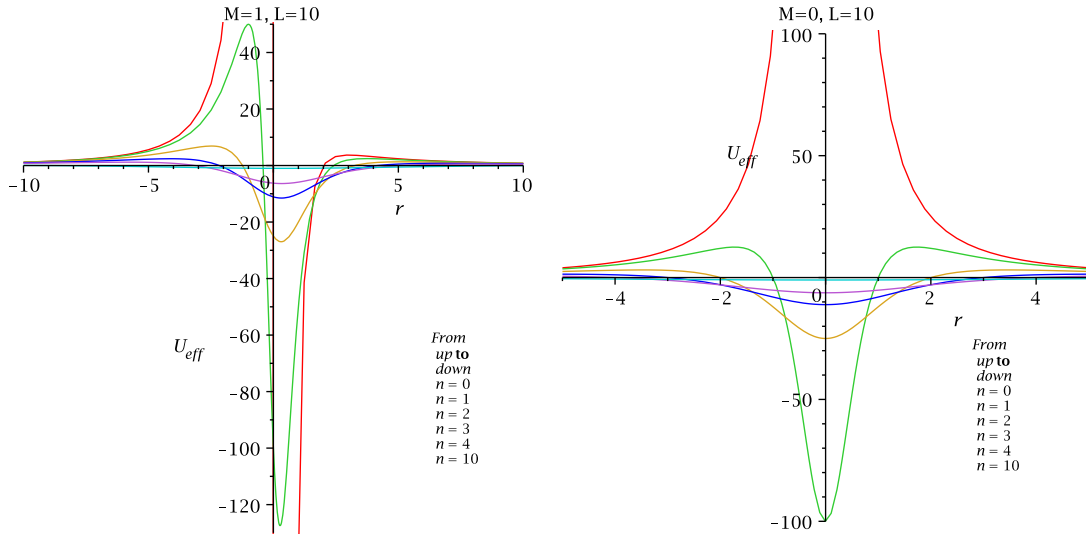


Figure 12: The figure shows the variation of  $U_{eff}$  with  $r$  for TN BH and mass-less TN BH.

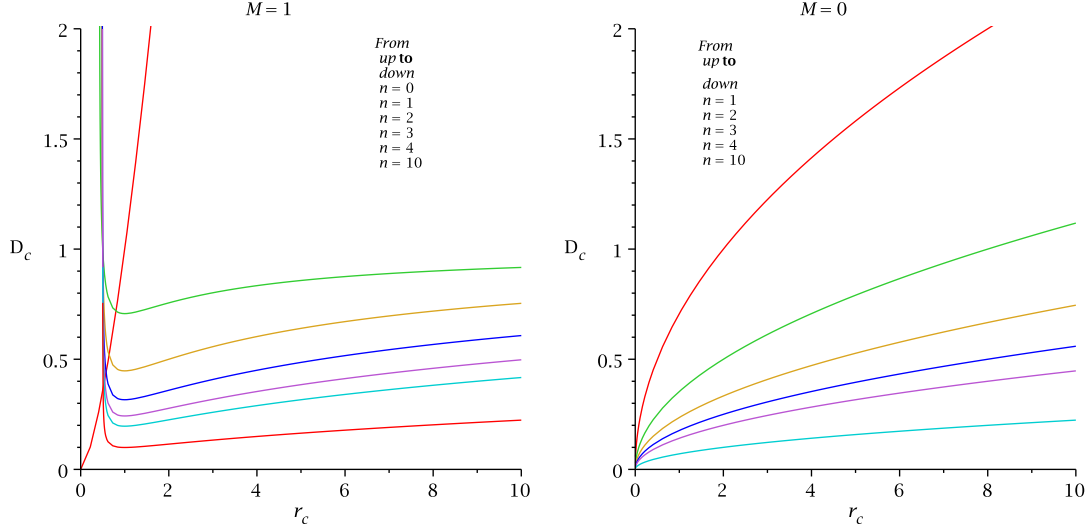


Figure 13: The figure shows the variation of  $D_c$  with  $r_c$  for TN BH and mass-less TN BH.

The behaviour of the impact parameter can be shown from the Fig. 13. Putting the Eq. (18) in Eq. (16), we obtain the equation of CPO [18, 27]:

$$r_c^3 - 3Mr_c^2 - 3n^2r_c + Mn^2 = 0. \quad (19)$$

For mass-less TN BH[18], the root of the Eq. becomes

$$r_c = \pm\sqrt{3}n. \quad (20)$$

The variation of CPO with  $r_c$  for TN BH and mass-less TN BH could be found in the Fig. 13.

The gravitational bending of light analyzed in [16] and the bending angle on the cone is computed in [16]  $\alpha = \frac{4M}{D}$ . In terms of opening angle it should be  $\alpha = \frac{2M\delta}{n}$ . For *massless TN spacetime*, this angle reduces to zero value.

### 3.2 Circular Time-like Geodesics:

For time-like geodesic we have to set  $\epsilon = -1$  then the effective potential becomes

$$V_{eff} = \left( \frac{r^2 - 2Mr - n^2}{r^2 + n^2} \right) \left( 1 + \frac{L^2}{r^2 + n^2} \right). \quad (21)$$

The qualitative behaviour of the test particle could be obtained by studying this potential. First we consider the zero angular momentum geodesics for this the effective potential

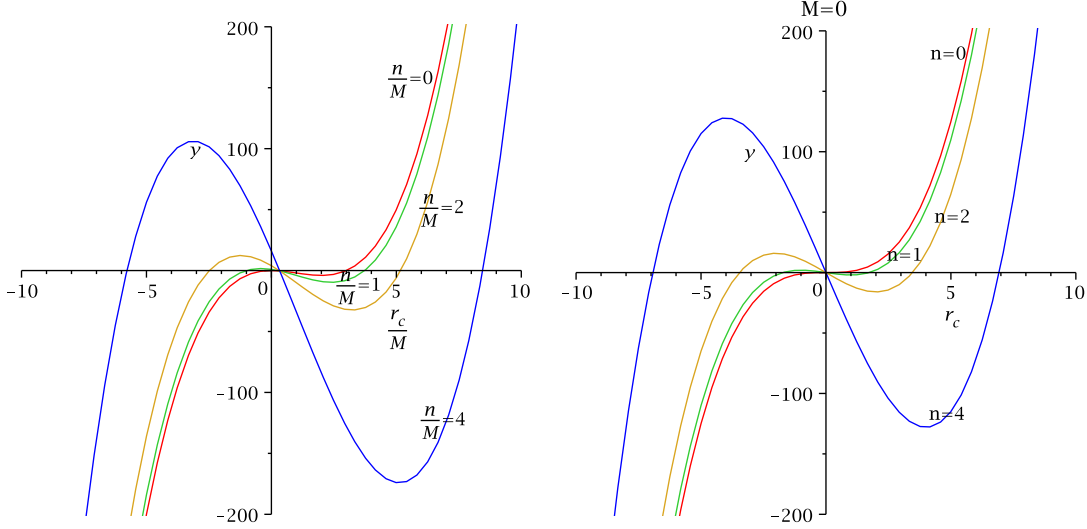


Figure 14: The stability threshold is defined by the largest real root of the cubic  $y = r_c^3 - 3Mr_c^2 - 3n^2r_c + Mn^2 = 0$ . For mass-less case,  $y = r_c^3 - 3n^2r_c = 0$ . For  $n = 0$  this root has the value  $r_c = 3M$ .

reduces to

$$V_{eff} = \left( \frac{r^2 - 2Mr - n^2}{r^2 + n^2} \right). \quad (22)$$

One can observe the qualitative behaviour of the geodesics in the presence of dual mass and with out dual mass and also mass-les. This could be seen from the Fig. 15. In this plot we can see that the presence of the dual mass deforms the shape of the radial effective potential in comparison with zero dual mass. This behaviour also could be seen from the mass-less case.

For  $L \neq 0$ , the behaviour of the test particle in the potential well could be seen from the following Fig. 16, Fig. 17, Fig. 18, 19, 20, Fig. 21, Fig. 22 and Fig. 23.

In the above figures, we have seen that the radial dependency of the effective potential with dual mass, without dual mass and  $M = 0$ . When  $n = 0$ , the effective potential at large radial distance do not change much more with the increasing of  $L$ . When we introduced the NUT parameter, the shape of the effective potential *deforms* in comparison with NUT less case and it also changes for different values of angular momentum. Finally, when we increase the value of  $n$  the height of the potential well decreases. This work has been done earlier for the parameter  $a$ ,  $Q$  and  $n$ . This work is specially for  $a = Q = 0$  and mass-less cases which has been not studied previously.

Now re-write the Eq. 13 for time-like geodesics as

$$\dot{r}^2 (r^2 + n^2)^2 = (E^2 - 1) (r^2 + n^2)^2 + 2Mr (r^2 + n^2) - L^2 (r^2 - 2Mr - n^2)$$

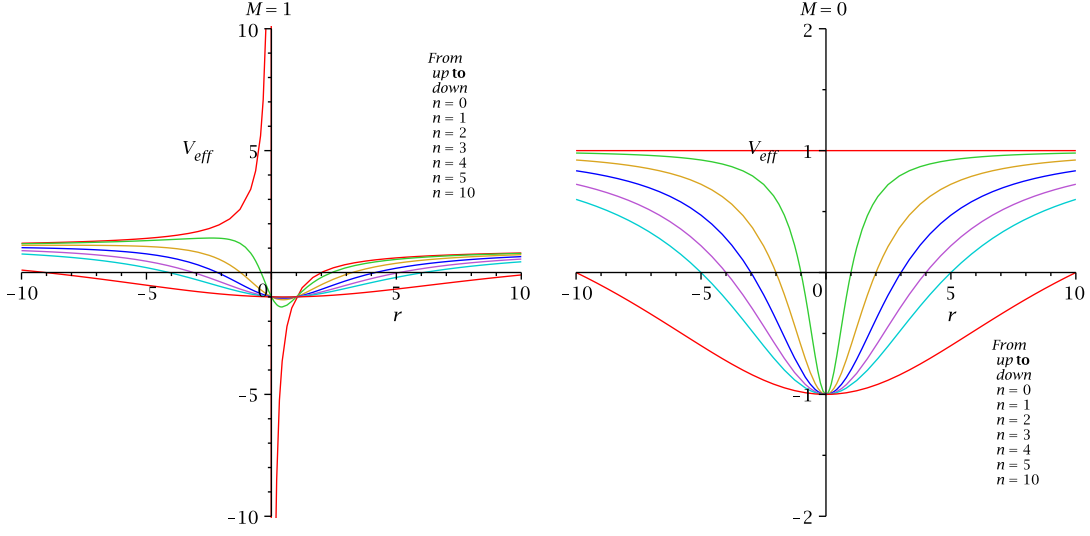


Figure 15: The figure shows the variation of  $V_{eff}$  with  $r$  for TN BH and mass-less TN BH.

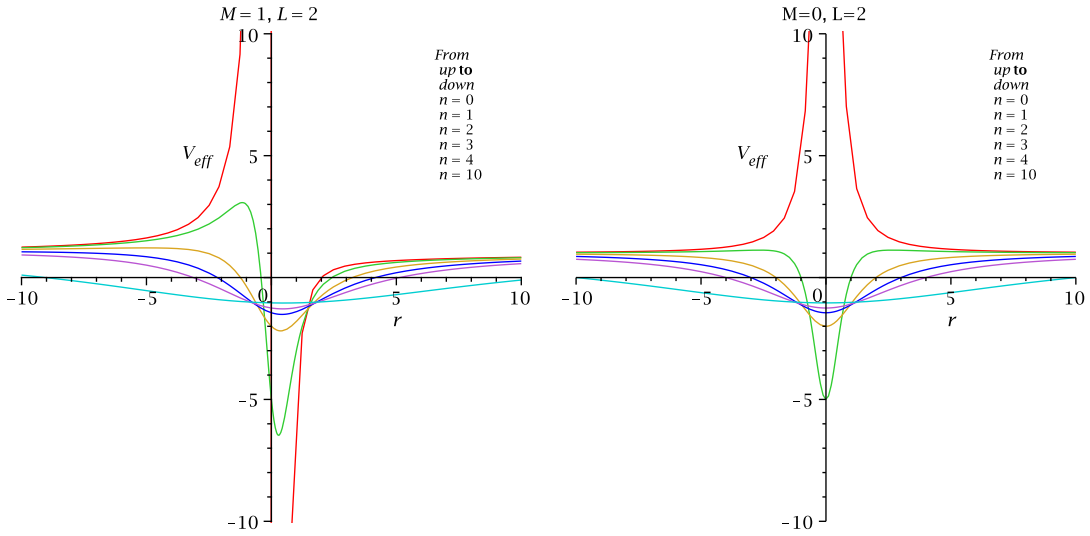


Figure 16: The figure shows the variation of  $V_{eff}$  with  $r$  for for TN BH and mass-less TN BH.

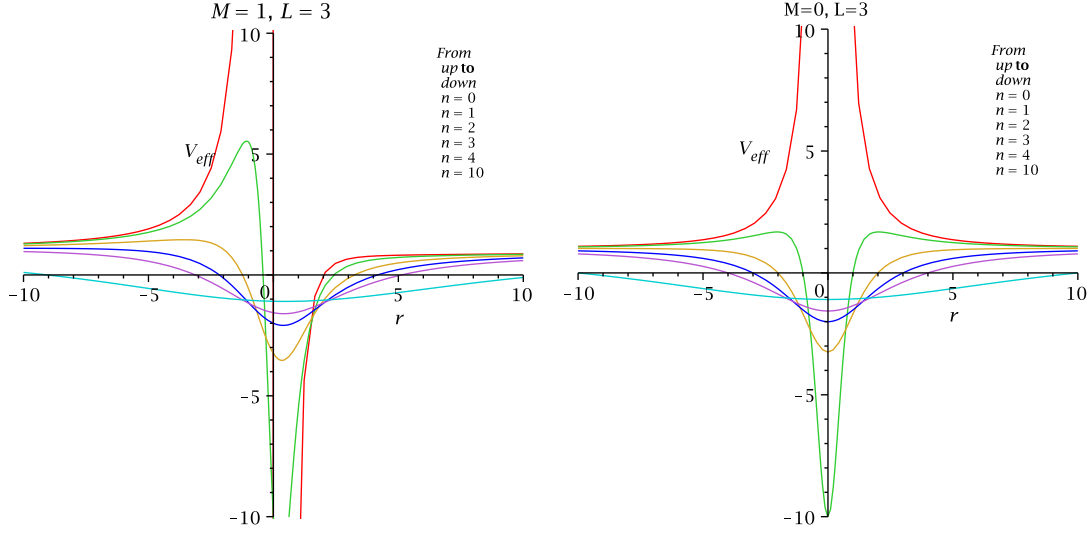


Figure 17: The figure shows the variation of  $V_{eff}$  with  $r$  for for TN BH and mass-less TN BH. NUT parameter.

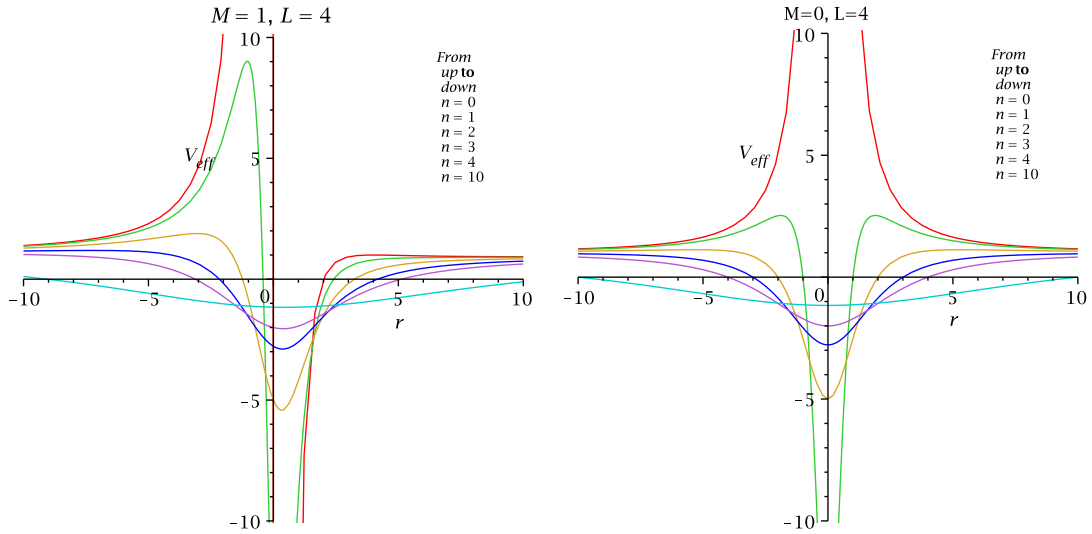


Figure 18: The figure shows the variation of  $V_{eff}$  with  $r$  for TN BH and mass-less TN BH.



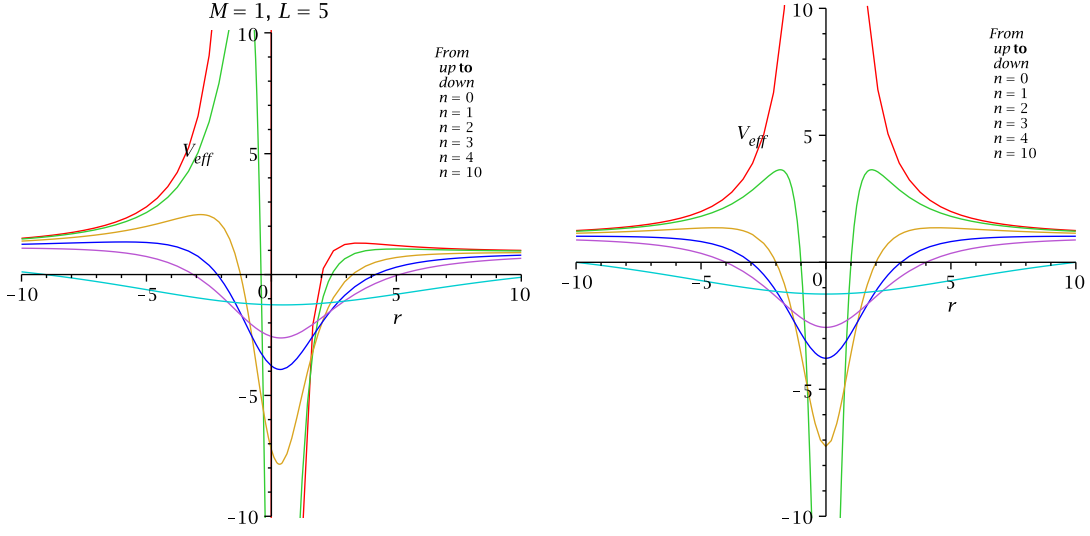


Figure 19: The figure shows the variation of  $V_{eff}$  with  $r$  for TN BH and mass-less TN BH.

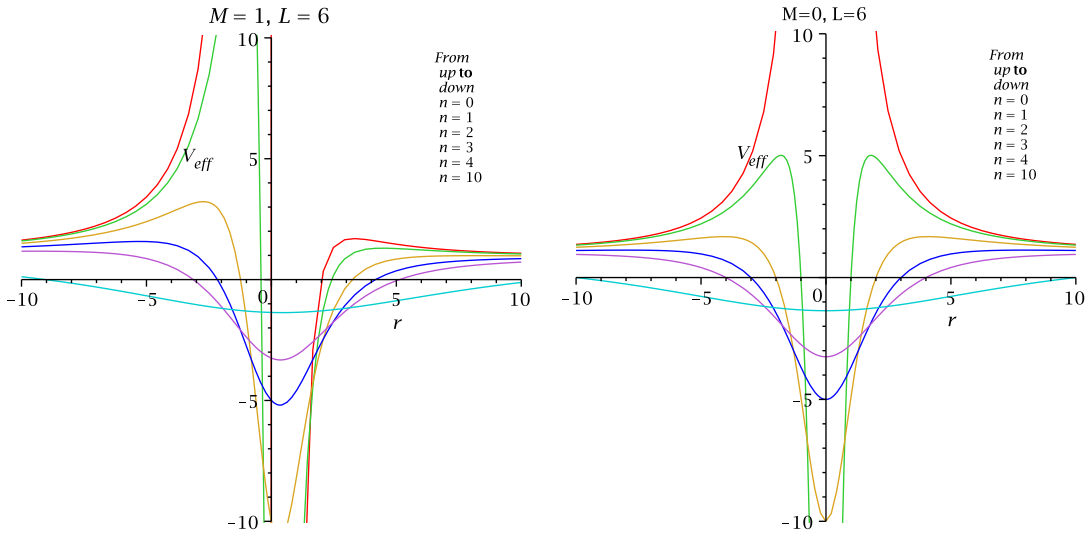


Figure 20: The figure shows the variation of  $V_{eff}$  with  $r$  for for TN BH and mass-less TN BH.

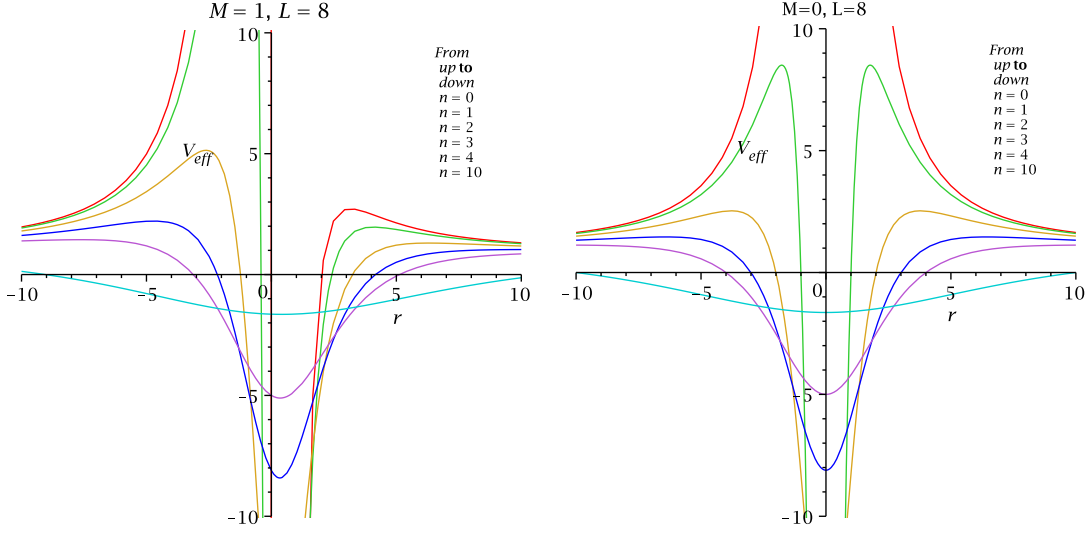


Figure 21: The figure shows the variation of  $V_{eff}$  with  $r$  for TN BH and mass-less TN BH.

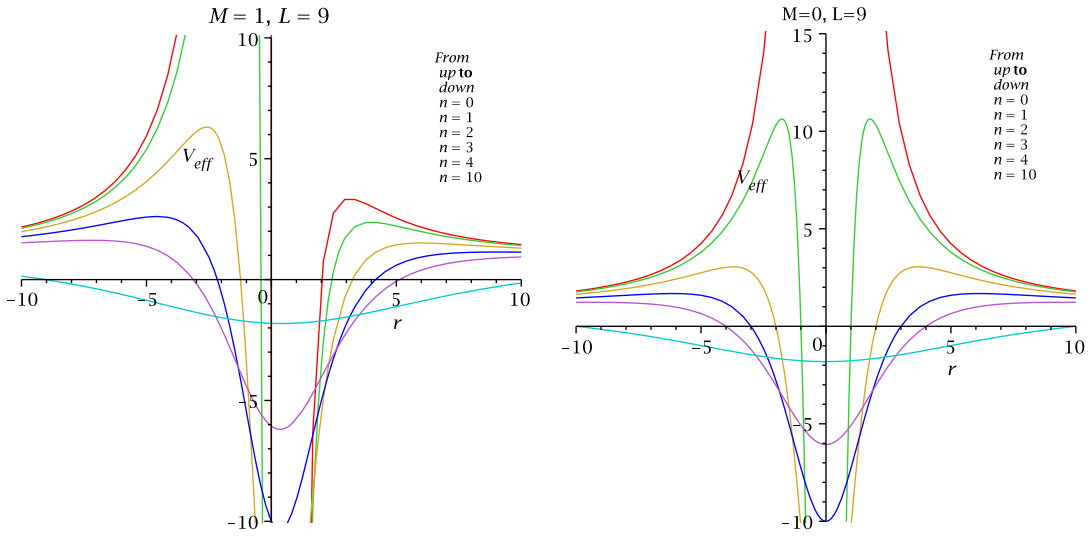


Figure 22: The figure shows the variation of  $V_{eff}$  with  $r$  for TN BH and mass-less TN BH.

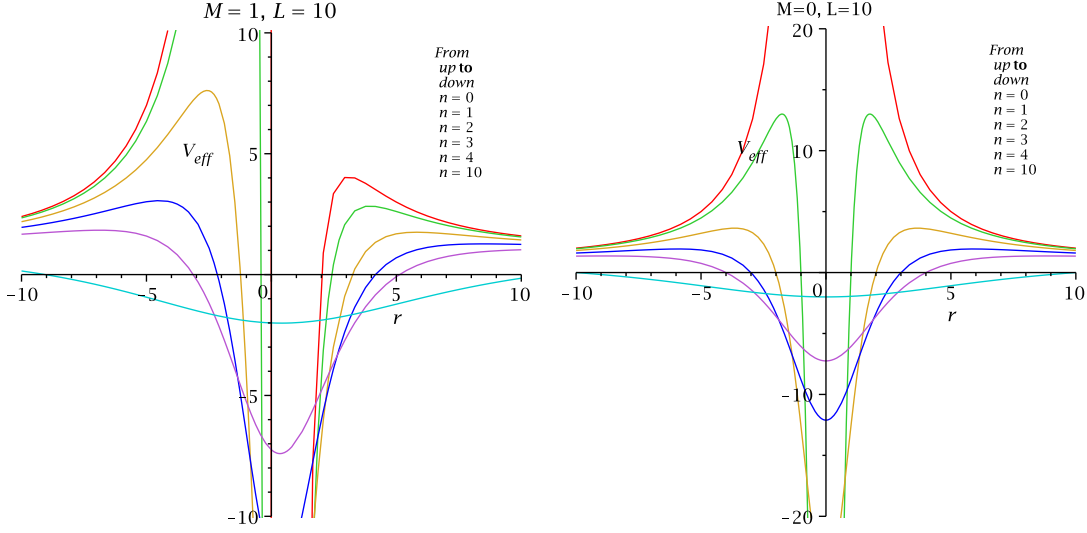


Figure 23: The figure shows the variation of  $V_{eff}$  with  $r$  for TN BH and mass-less TN BH.

$$+ 2n^2(r^2 + n^2) . \quad (23)$$

For circular geodesics  $r = r_0$ , we have the following condition:

$$\dot{r}^2|_{r=r_0} = \frac{d\dot{r}^2}{dr}|_{r=r_0} = 0 . \quad (24)$$

From this condition, we find the energy and angular momentum for circular orbit:

$$E_0^2 = \frac{r_0(r_0^2 - 2Mr_0 - n^2)^2}{(r_0^2 + n^2)(r_0^3 - 3Mr_0^2 - 3n^2r_0 + Mn^2)} . \quad (25)$$

and

$$L_0^2 = \frac{(r_0^2 + n^2)(Mr_0^2 + 2n^2r_0 - Mn^2)}{(r_0^3 - 3Mr_0^2 - 3n^2r_0 + Mn^2)} . \quad (26)$$

These equations require for energy square and angular momentum square positive definite i.e.  $r_0^3 - 3Mr_0^2 - 3n^2r_0 + Mn^2 > 0$ . Compare with the Eq. 19 it implies that the minimum radius for time-like circular orbit is the radius of the unstable CPO. Interestingly for mass-less case, these values are

$$E_0^2 = \frac{(r_0^2 - n^2)^2}{(r_0^2 + n^2)(r_0^3 - 3n^2r_0)} . \quad (27)$$

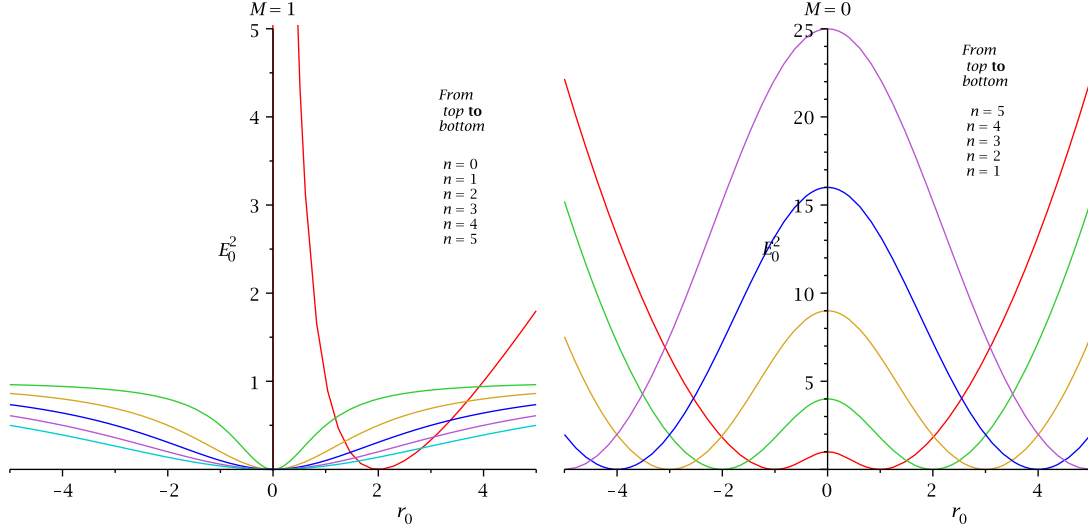


Figure 24: The figure depicts the variation of  $E_0^2$  with  $r_0$  for TN BH and mass-less TN BH.

and

$$L_0^2 = \frac{2n^2(r_0^2 + n^2)}{(r_0^2 - 3n^2)}. \quad (28)$$

We have plotted their behaviour in the Fig. 24 and Fig. 25. and

From Eq. 23, and for circular orbit we obtain

$$L_{\pm} = \pm \sqrt{\frac{(E^2 - 1)(r_0^2 + n^2)^2 + 2Mr_0(r_0^2 + n^2) + 2n^2(r_0^2 + n^2)}{r_0^2 - 2Mr_0 - n^2}}. \quad (29)$$

It should be noted that  $L_+ = -L_-$ . From this expression, it follows that the angular momentum parameter explicitly depends upon the energy value. Therefore there must be difference in the circular orbits in the  $L - r$  plane for  $E^2 > 1$ ,  $E^2 < 1$  and  $E^2 = 1$ . We are interested here to look the behaviour of the circular geodesics in this plane by incorporating these energy conditions.

When  $E^2 < 1$ , we obtain the bound orbits, this can be displayed from the  $L_+ - r_0$  diagram. It has been shown in the Fig. 26. For  $E^2 = 1$ , we find the marginally escape orbits. This has been seen from the Fig. 27. Finally for  $E^2 > 1$ , we find the unbound orbits. This could be seen from the Fig. 28, Fig. 29 and Fig. 30.

Now we see the behaviour of the  $L$  with  $r$  for different values of energy for a fixed value of the dual mass.

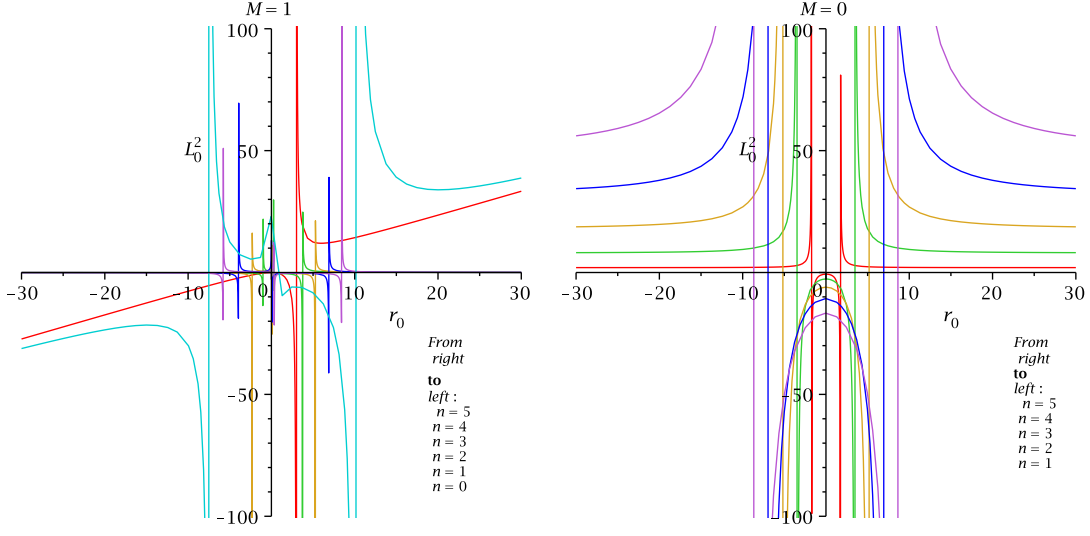


Figure 25: The figure depicts the variation of  $E_0^2$  with  $r_0$  for TN BH and mass-less TN BH.

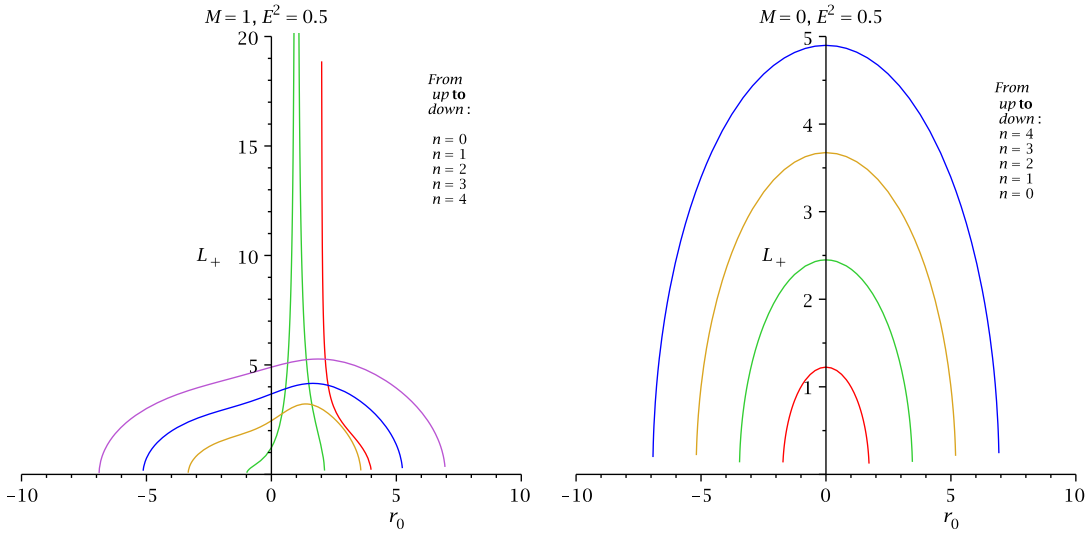


Figure 26: The figure shows the variation of  $L_+$  with  $r_0$  for TN BH and mass-less TN BH.

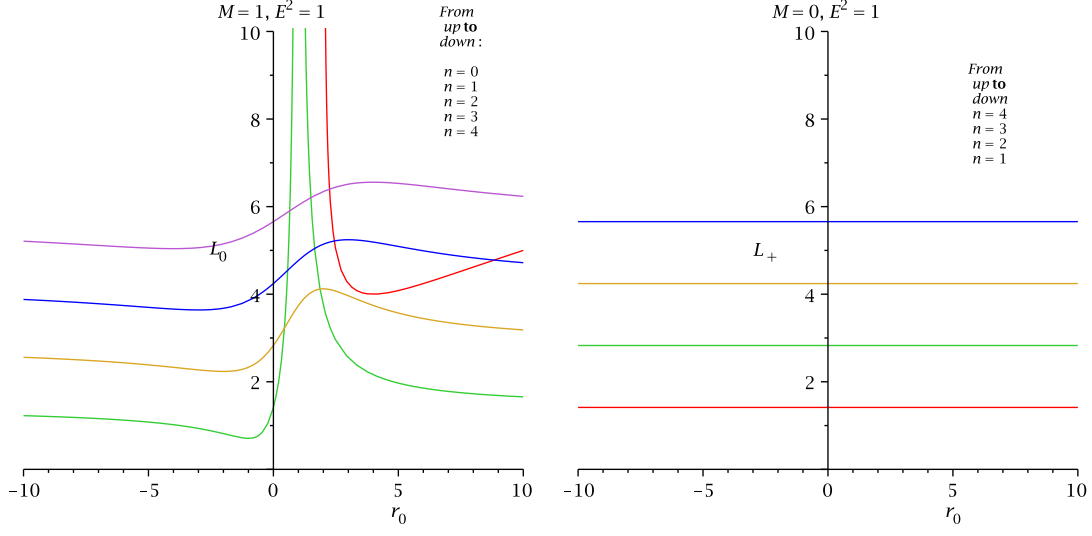


Figure 27: The figure shows the variation of  $L_+$  with  $r_0$  for TN BH and mass-less TN BH.

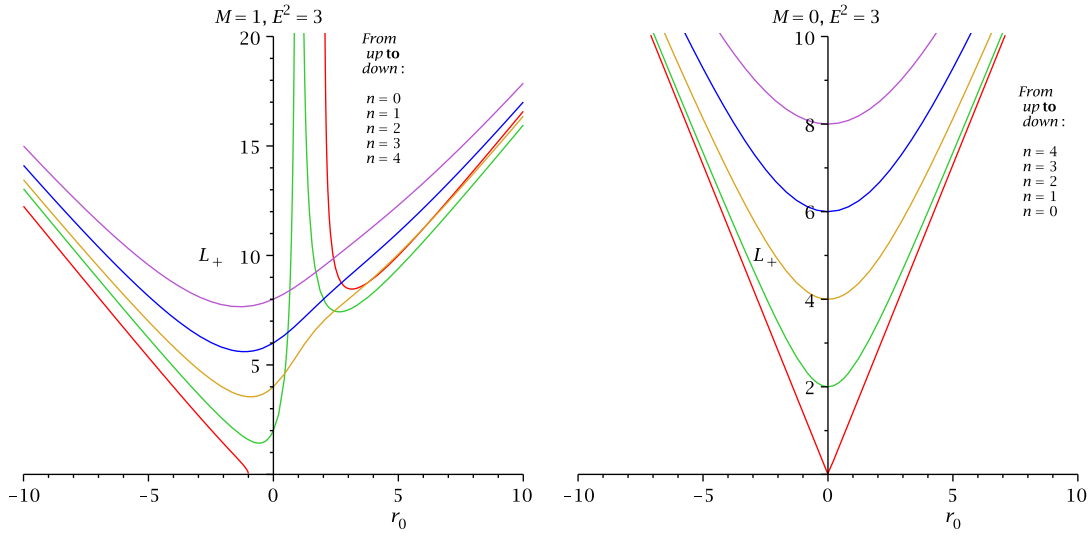


Figure 28: The figure shows the variation of  $L_+$  with  $r_0$  for TN BH and mass-less TN BH.

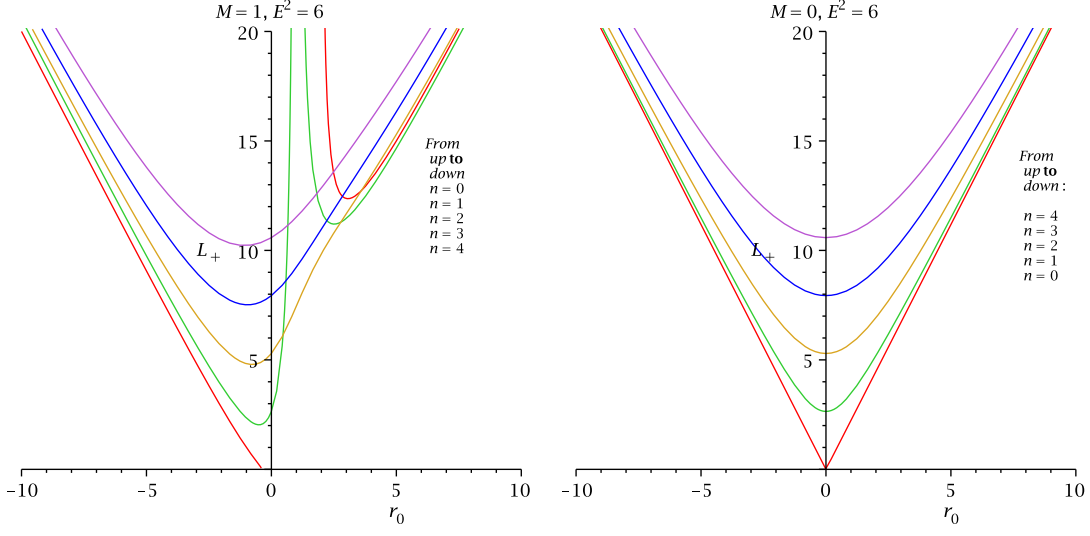


Figure 29: The figure shows the variation of  $L_+$  with  $r_0$  for TN BH and mass-less TN BH.

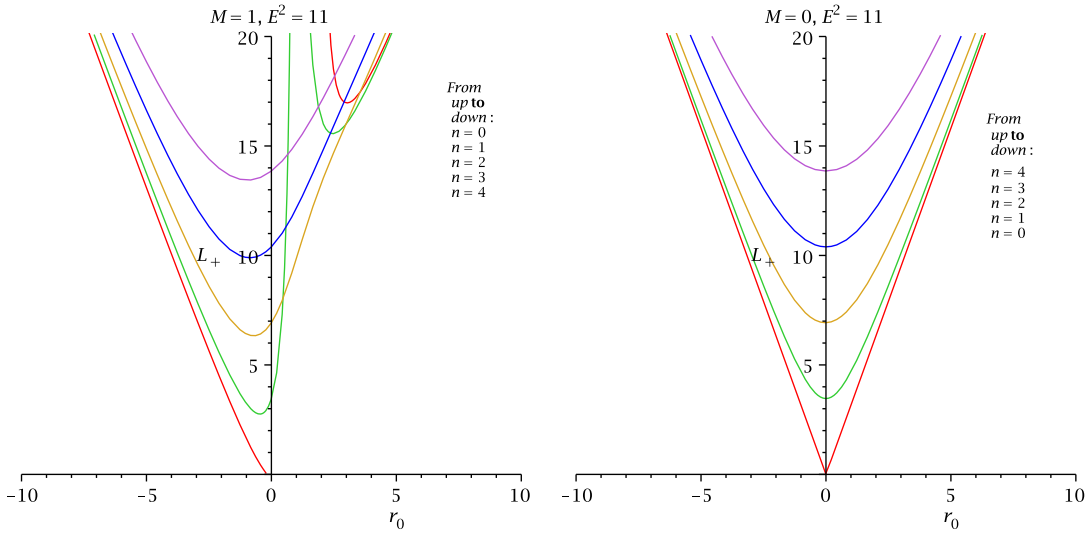


Figure 30: The figure shows the variation of  $L_+$  with  $r_0$  for TN BH and mass-less TN BH.

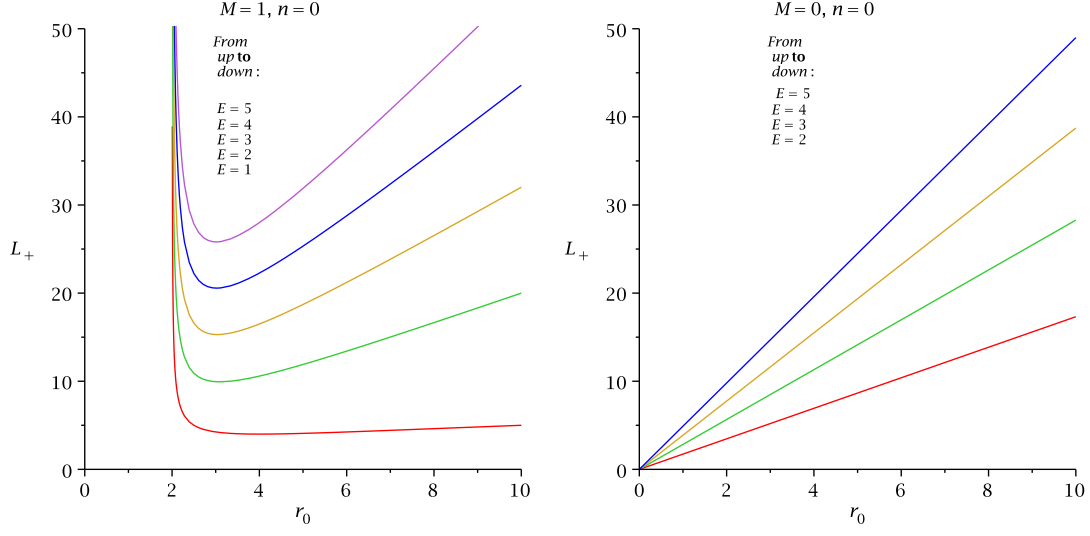


Figure 31: The figure depicts the variation of  $L_+$  with  $r_0$  for TN BH and mass-less TN BH.

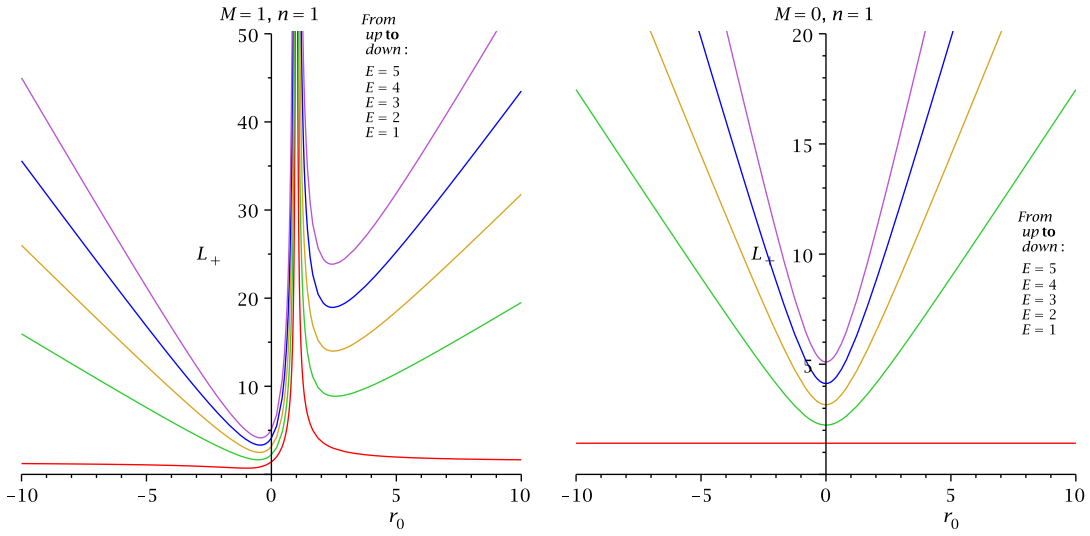


Figure 32: The figure depicts the variation of  $L_+$  with  $r_0$  for TN BH and mass-less TN BH.



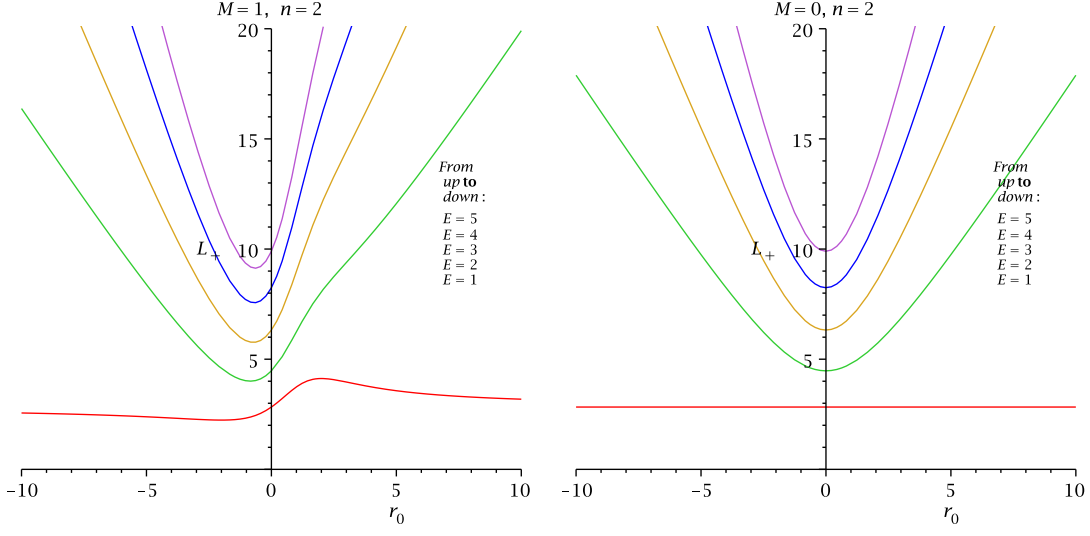


Figure 33: The figure depicts the variation of  $L_+$  with  $r_0$  for TN BH and mass-less TN BH.

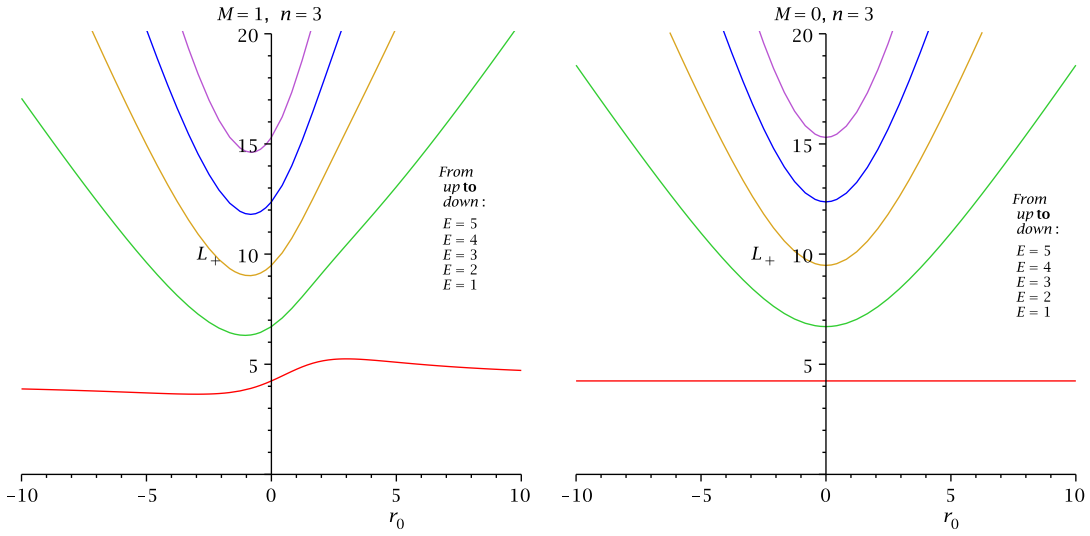


Figure 34: The figure depicts the variation of  $L_+$  with  $r_0$  for TN BH and mass-less TN BH.

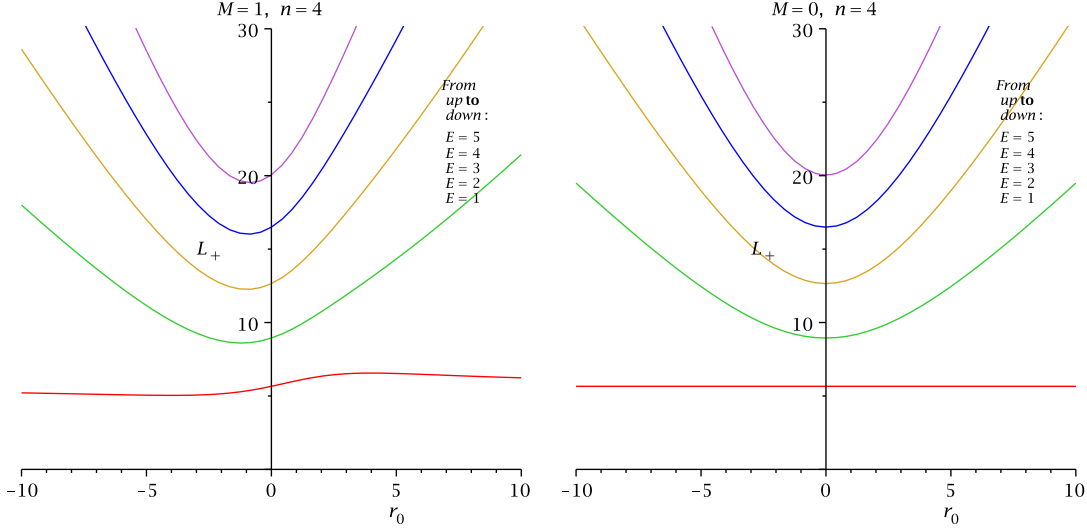


Figure 35: The figure depicts the variation of  $L_+$  with  $r_0$  for TN BH and mass-less TN BH.

Now the ISCO radius can be obtained using the condition Eq. 24 with additional condition:

$$\left. \frac{d^2 r^2}{dr^2} \right|_{r=r_0} = 0. \quad (30)$$

Although it has been derived earlier in [27]. We are interested here to see the behaviour of ISCO in the presence of NUT parameter and with out NUT parameter in comparison with mass-less cases in more graphically which has been not shown there. Therefore the ISCO equation for TN BH could be obtain by applying the condition Eq. 24 and Eq. 30 (or by putting  $a = Q = 0$  in Eq. (81) in [27]):

$$\begin{aligned} Mr_0^6 - 6M^2r_0^5 - 15Mn^2r_0^4 + (4M^2n^2 - 16n^4)r_0^3 + \\ 15Mn^4r_0^2 - 6M^2n^4r_0 - Mn^6 = 0. \end{aligned} \quad (31)$$

and for the mass-less TN BH, it is

$$r_0 = 0. \quad (32)$$

and it also indicates there is *no ISCO for massless TN BH*. It is a curious result although there exists mass-less CPO. The variation of ISCO in the presence of the NUT parameter and without NUT parameter could be found in the Fig. 36.

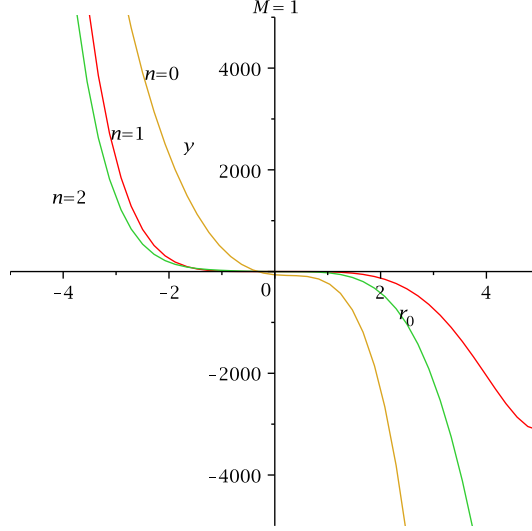


Figure 36: The figure depicts the variation of ISCO with  $r_0$  in the presence of NUT parameter and without NUT parameter. Where  $y = Mr_0^6 - 6M^2r_0^5 - 15Mn^2r_0^4 + (4M^2n^2 - 16n^4)r_0^3 + 15Mn^4r_0^2 - 6M^2n^4r_0 - Mn^6$ .

### 3.3 MBCO:

Another interesting orbit that has not been considered previously in [18] but considered in [27] for KNTN BH. So we have just set  $E_0^2 = 1$  in EQ. 25 (or putting the parameters  $a = Q = 0$  in Eq. (98) in [27] ), we find the MBCO for TN BH:

$$Mr_0^7 - 4M^2r_0^6 - 7Mn^2r_0^5 + (2M^2n^2 - 4n^4)r_0^4 + (M^2n^4 - 4n^6)r_0^2 + 4Mn^6r_0 - M^2n^6 = 0. \quad (33)$$

and for the mass-less TN BH, it is

$$r_0^2 + n^2 = 0. \quad (34)$$

It implies that there is no existence of MBCO for mass-less case. From Eq. 33, in the limit  $n = 0$ , we get the MBCO for Schwarzschild BH[26]. In Fig. 37, we have plotted the MBCO with  $r_0$  in comparison with Schwarzschild BH.

## 4 Geodesics in Extreme TN Spacetime:

In the previous section, we have discussed the complete geodesic structure for non-extreme TN BH. Moreover, we have clearly explained the difference of geodesic structure between

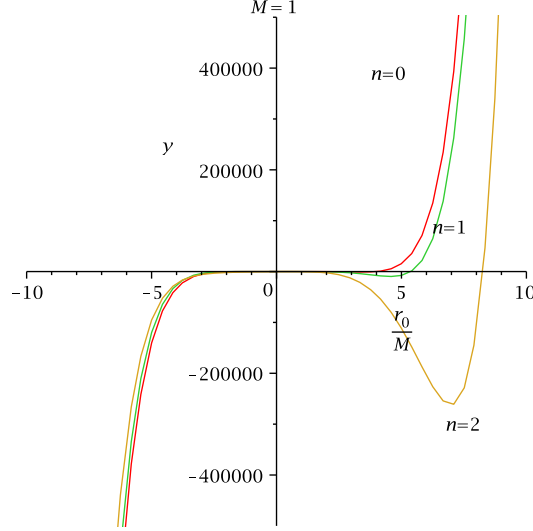


Figure 37: Here  $y = Mr_0^7 - 4M^2r_0^6 - 7Mn^2r_0^5 + (2M^2n^2 - 4n^4)r_0^4 + (M^2n^4 - 4n^6)r_0^2 + 4Mn^6r_0 - M^2n^6$ .

TN spacetime and mass-less TN spacetime in graphically. In the present section we shall discuss more interesting case i.e. *extreme TN* spacetime. What happens the geodesic structure in the extreme limit i.e.  $r_+ = r_-$ . This is the main aim in this section. Proceeding similarly, we can write the effective potential for massive particles in the extreme limit (using Eq. 21) given by

$$V_{eff} = \left( \frac{r-M}{r+M} \right) \left( 1 + \frac{L^2}{r^2 - M^2} \right). \quad (35)$$

The qualitative behaviour of the test particle may be seen from the effective potential diagram (See Fig. 38).

Proceeding analogously, we apply for circular geodesics  $r = r_0$ , one obtains the energy and angular momentum for extreme TN BH (using Eq. 25 and Eq. 26):

$$E_0 = \sqrt{\frac{r_0}{r_0 + M}}. \quad (36)$$

and

$$L_0 = \sqrt{M(r_0 + M)}. \quad (37)$$

How  $E_0$  and  $L_0$  are varied with  $r_0$ , it can be seen from the Fig. 39 Now we have derived the ISCO equation for non-extreme TN BH but here we will see what would be the ISCO

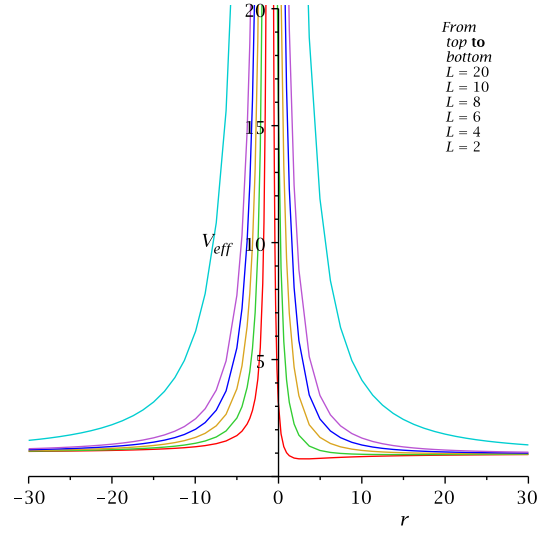


Figure 38: The variation of  $V_{eff}$  with  $r$  for extreme TN BH, Here  $M = 1$ .

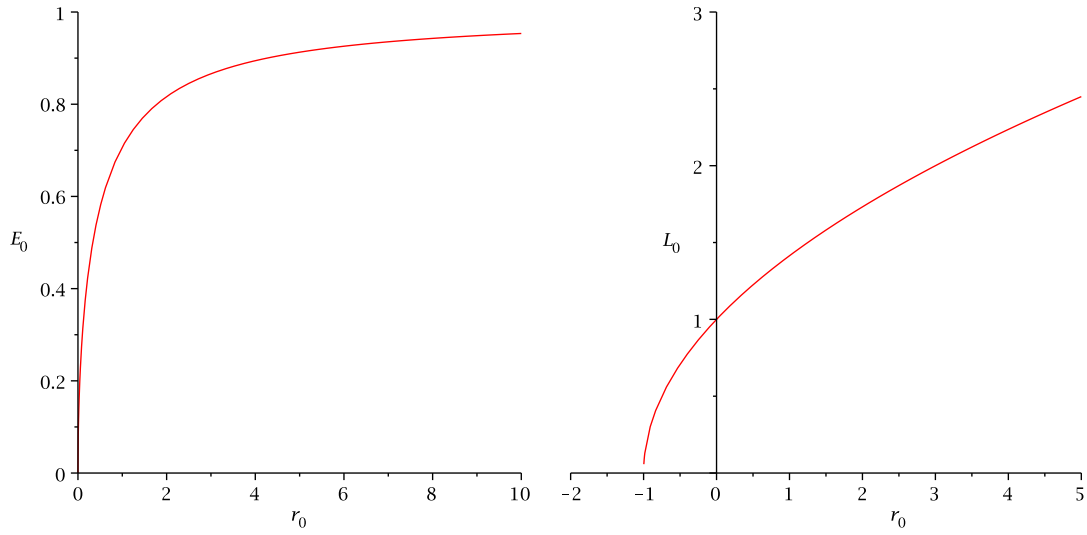


Figure 39: The variation of energy and angular momentum with  $r_0$  for extreme TN BH, Here  $M = 1$ .

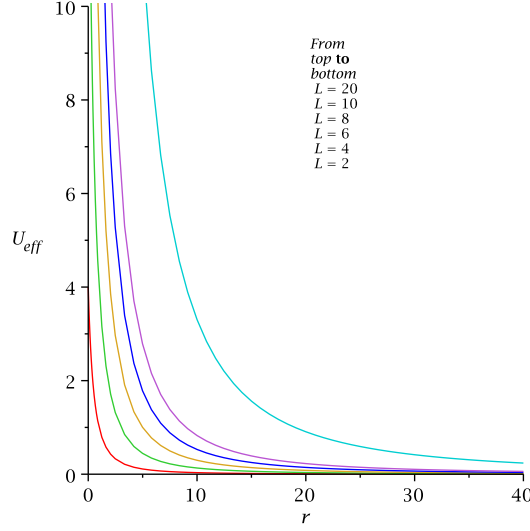


Figure 40: The variation of  $U_{eff}$  with  $r$  for extreme TN BH, Here  $M = 1$ .

radius in the extremal limit which is most important class of circular orbit in astrophysics. We find for extreme TN BH the ISCO radius (using Eq. 31) should be

$$r_0 = r_{isco} = M . \quad (38)$$

The corresponding ISCO energy and ISCO angular momentum are

$$E_{isco} = \frac{1}{\sqrt{2}} . \quad (39)$$

$$L_{isco} = \sqrt{2}M . \quad (40)$$

For photons, the effective potential in the extreme limit (using Eq. 15) reduces to

$$U_{eff} = \frac{L^2}{(r + M)^2} . \quad (41)$$

Its behaviour for different values of angular momentum can be seen from the Fig 40. Therefore, one obtains the CPO (using Eq. 19) for extreme TN BH:

$$r_c = r_{cpo} = M . \quad (42)$$

Similarly, we can find the radius of MBCO (using Eq. 33) for extreme TN BH:

$$r_0 = r_{mbco} = M . \quad (43)$$

Interestingly, we observed that for extreme TN BH the three radii namely ISCO, MBCO and CPO coincides with the horizon i.e.

$$r_{isco} = r_{mbco} = r_{cpo} = M . \quad (44)$$

This has not been previously examined in the literature that for extreme TN BH three orbits are coincident with the Killing horizons i.e. null geodesic generators of the horizon. First spherically symmetric extreme string BH this result has been observed in [33]. Probably, this is a *first* example for any spherically symmetric, stationary and non-asymptotic extreme spacetime that possesses such feature.

## 5 Discussion:

In this paper we examined the geodesic motion of test particles in the background geometry of TN spacetime in comparison with mass-less (zero mass) TN spacetime. We considered the both massive and mass-less test particles case. We differentiated the ISCO, MBCO and CPO in graphically between TN spacetime and mass-less TN spacetime. From effective potential diagram we showed the presence of the NUT parameter changes the shape of the potential well in comparison with zero NUT parameter and mass-less spacetime. We studied the circular orbits in the  $L - r$  plane for different values of energy i.e.  $E^2 > 1$ ,  $E^2 < 1$  and  $E^2 = 1$  in case of TN and mass-less TN spacetime.

We also derived the geodesic motion of test particles (both massive and mass-less) in case of extreme TN BH. Interestingly, we showed that the three radii i.e. the radius of ISCO, the radius of MBCO and the radius of CPO are coincident with the Killing horizon radius. This is very surprising result because probably we first obtained this result for any spherically symmetric, stationary and non-asymptotic spacetime.

## A Centre of Mass Energy of Particle Collision near the horizon of TN BH:

In this section, we should study what is the role of NUT parameter in the BSW effect which was predicted by Bañados, Silk and West [32] several years ago. Does TN BH could be act as a particle accelerator with arbitrarily high energy when the BH is extremal. This is the main aim in this section motivated by the previous section from the analysis of geodesic structure. We have considered the particle acceleration and collision in the Centre-of-Mass (CM) frame. To determine the CM energy, we consider first two particles coming from infinity with  $\frac{\mathcal{E}_1}{m_0} = \frac{\mathcal{E}_2}{m_0} = 1$  approaching the TN BH with different angular momenta  $L_1$  and  $L_2$  and colliding at some radius  $r$ . Later, we choose the collision point is at  $r$  to approach the horizon  $r = r_+$ . Also we have assumed that the particles are initially to be at rest at infinity.

The formula that we have used here suggested first by BSW [32] should read

$$\left(\frac{\mathcal{E}_{cm}}{\sqrt{2}m_0}\right)^2 = 1 - g_{\mu\nu}u_1^\mu u_2^\nu. \quad (45)$$

Since in the previous section we have calculated total geodesic structure confined in the equatorial plane for TN BH, so we should not repeat them again. Due to the time-like isometry and space-like isometry the space-time possesses two conserved quantities one is energy and other is angular momentum. Thus for massive particles, the components of the four velocity are

$$u^t = \dot{t} = \frac{\mathcal{E}}{\mathcal{H}(r)} \quad (46)$$

$$u^r = \dot{r} = \pm \sqrt{\mathcal{E}^2 - \mathcal{H}(r) \left(1 + \frac{L^2}{r^2 + n^2}\right)} \quad (47)$$

$$u^\theta = \dot{\theta} = 0 \quad (48)$$

$$u^\phi = \dot{\phi} = \frac{L}{r^2 + n^2}. \quad (49)$$

and

$$u_1^\mu = \left(\frac{\mathcal{E}_1}{\mathcal{H}(r)}, -X_1, 0, \frac{L_1}{r^2 + n^2}\right). \quad (50)$$

$$u_2^\mu = \left(\frac{\mathcal{E}_2}{\mathcal{H}(r)}, -X_2, 0, \frac{L_2}{r^2 + n^2}\right). \quad (51)$$

Putting these value in (45), we find the expression for CM energy:

$$\left(\frac{\mathcal{E}_{cm}}{\sqrt{2}m_0}\right)^2 = 1 + \frac{\mathcal{E}_1\mathcal{E}_2}{\mathcal{H}(r)} - \frac{X_1X_2}{\mathcal{H}(r)} - \frac{L_1L_2}{r^2 + n^2}. \quad (52)$$

where,

$$X_1 = \sqrt{\mathcal{E}_1^2 - \mathcal{H}(r) \left(1 + \frac{L_1^2}{r^2 + n^2}\right)}, \quad X_2 = \sqrt{\mathcal{E}_2^2 - \mathcal{H}(r) \left(1 + \frac{L_2^2}{r^2 + n^2}\right)}$$

For simplicity,  $\mathcal{E}_1 = \mathcal{E}_2 = 1$  and reverting back the value of  $\mathcal{H}(r)$ , we obtain the CM energy near the event horizon ( $r_+$ ) of TN space-time:

$$\mathcal{E}_{cm} |_{r \rightarrow r_+} = \sqrt{2}m_0 \sqrt{\frac{4(r_+^2 + n^2) + (L_1 - L_2)^2}{2(r_+^2 + n^2)}}. \quad (53)$$



and for Cauchy horizon ( $r_-$ ) the CM energy is

$$\mathcal{E}_{cm} |_{r \rightarrow r_-} = \sqrt{2}m_0 \sqrt{\frac{4(r_-^2 + n^2) + (L_1 - L_2)^2}{2(r_-^2 + n^2)}}. \quad (54)$$

where  $r_{\pm}$  is defined previously. It implies that the CM energy is finite and depends upon the values of angular momentum parameter. It also suggests that the CM energy depends upon the NUT parameter. It may also playing a key role in the BSW effect as we have seen from the above expression.

In the limit  $n = 0$ , the above expression reduces to the following form

$$\mathcal{E}_{cm} = \sqrt{2}m_0 \sqrt{\frac{16M^2 + (L_1 - L_2)^2}{8M^2}}. \quad (55)$$

which is exactly CM energy of the Schwarzschild BH found by BSW in [32].

Now see what happens in case of mass-less case and *extreme* case? First we consider the mass-less case, in this case the CM energy is given by

$$\mathcal{E}_{cm} |_{r \rightarrow r_{\pm}} = \sqrt{2}m_0 \sqrt{\frac{8n^2 + (L_1 - L_2)^2}{4n^2}}. \quad (56)$$

It indicates that the CM energy is finite depends on the NUT parameter. More interesting case i.e the extreme case where the CM energy is given by

$$\mathcal{E}_{cm} |_{r \rightarrow M} = \sqrt{2}m_0 \sqrt{\frac{4(M^2 + n^2) + (L_1 - L_2)^2}{2(M^2 + n^2)}}. \quad (57)$$

Since we know for extreme case,  $r_+ = r_- = M$  and  $M^2 + n^2 = 0$ . Therefore we find for extreme TN BH:

$$\mathcal{E}_{cm} |_{r \rightarrow M} \rightarrow \infty. \quad (58)$$

i.e the CM energy is *divergent*. This is an amusing result. Because we first reported a non-asymptotic, spherically symmetric and stationary extreme BH spacetime possesses such properties.

## B Null Circular Geodesics and QNM for TN BH in the Eikonal approximation:

In this appendix section, we should study another interesting feature of NUT spacetime that is QNM in the “eikonal approximation”. This term first used by Mashhoon in 1985 [34] where the author studied the stability of spinning charged BH by using this technique.

Subsequently, Cardoso et al. [35] showed in 2009 the QNM frequency of the null circular geodesics in the the eikonal limit which is related to the Lyapunov exponent and which determines the instability time scale of the circular orbit.

Let us briefly derive the QNM frequency for TN BH in the eikonal limit following the work by [35]. It has been shown by the author in [36] that the unstable CPO is very useful to determining the characteristic modes of BH, which is known as QNM frequency. We do not discussed the derivation of this particular frequency here rather we write the explicit formula derived in [35]:

$$\omega_{QNM} = \ell \Omega_c - i \left( n + \frac{1}{2} \right) \lambda_c . \quad (59)$$

where  $n$  is the overtone number,  $\ell$  is the angular momentum of the perturbation,  $\Omega_c$  is the angular frequency measured by the asymptotic observers and  $\lambda_c$  is the coordinate time Lyapunov exponent for null circular geodesics which defined in terms of the effective potential for null circular geodesics:

$$\lambda_c = \sqrt{-\frac{U''_{eff}}{2\dot{t}^2}} . \quad (60)$$

and

$$\Omega_c = \frac{\dot{\phi}}{\dot{t}} = \frac{1}{D_c} . \quad (61)$$

For TN BH,  $\Omega_c$  and  $\lambda_c$  are

$$\Omega_c = \sqrt{\frac{Mr_c^2 + 2n^2r_c - Mn^2}{r_c(r_c^2 + n^2)^2}} . \quad (62)$$

and

$$\lambda_c = \sqrt{\frac{3(2Mr_c + n^2 - r_c^2)(r_c^4 - 4Mr_c^3 - 6n^2r_c^2 + 4Mn^2r_c + n^4)}{(r_c^2 + n^2)^4}} . \quad (63)$$

Putting these values in the Eq. (61), one obtains the QNM frequency for TN BH in the eikonal limit.

For *massless* TN spacetime, the QNM frequency in the eikonal limit becomes

$$\omega_{QNM} = \ell \sqrt{2} \left( \frac{n}{r_c^2 + n^2} \right) - i \left( n + \frac{1}{2} \right) \sqrt{\frac{3(n^2 - r_c^2)(r_c^4 - 6n^2r_c^2 + n^4)}{(r_c^2 + n^2)^4}} \quad (64)$$

The physical significance of these frequencies are in the eikonal limit, the real and imaginary part of the QNMs of TN BH are given by the frequency and instability time scale of the unstable CPO. This is one of the key point of this work.

When the NUT parameter vanishes, one obtain the QNM frequency for Schwarzschild BH in the eikonal limit [37]:

$$\omega_{QNM} = \ell \sqrt{\frac{M}{r_c^3}} - i \left( n + \frac{1}{2} \right) \frac{\sqrt{3}M}{r_c^2} \quad (65)$$

## References

- [1] A. H. Taub, *Ann. of Maths.* **53**, 3 (1951).
- [2] E. Newman, L. Tamburino, T. Unti, *J. Math. Phys.* **4**, 7 (1963).
- [3] C. W. Misner and A. H. Taub, *Soviet Phys. JETP* **28**, 122 (1969).
- [4] A. Zee, *Phys. Rev. Lett.* **55**, 2379 (1985), and **56**, 1101(E) (1986).
- [5] S. Ramaswamy and A. Sen, *J. Math. Phys.* **22**, 11 (1981).
- [6] S. Ramaswamy and A. Sen, *Phys. Rev. Lett.* **57**, 1088 (1986).
- [7] J. S. Dowker and J. A. Roche, *Proc. of the Physical Society* **92** 575 (1967).
- [8] G. 't. Hooft, *Nucl. Phys.* **B79**, 276 (1974).
- [9] A. M. Polyakov, *JETP Lett.* **20**, 194 (1974).
- [10] P. A. M. Dirac, *Proc. Roy. Soc. London, ser. A* **133**, 60 (1931).
- [11] J. L. Friedman and R. D. Sorkin, *Phys. Rev. Lett.* **44**, 1100 (1980), and **45**, 148(E) (1980).
- [12] G. W. Gibbons and N. S. Manton, *Nucl. Phys.* **B274**, 183 (1986).
- [13] D. Lynden-Bell and M. Nouri-Zonoz, *Rev. Mod. Phys.*, 70, 427-445 (1998).
- [14] P. S. Letelier and W. M. Vieira, *Phys. Lett.*, A 244, 324 1998.
- [15] D. Vaman, M. Visinescu, *Phys. Rev. D* **54**, 1398 (1996).
- [16] D. Lynden-Bell, M. Nouri-Zonoz. *Mon. Not. R. Astron. Soc.* **292**, 714 (1997).
- [17] C. Liu, S. Chen, C. Ding and J. Jing, *Phys. Lett. B* **701**, 285 (2011).
- [18] C. Chakraborty, *Eur. Phys. J. C* **74**, 2759 (2014).
- [19] J. G. Miller, M. D. Kruskal, B. B. Godfrey, *Phys. Rev. D***4**, 2945 (1971).

- [20] P. Hajicek, *J. Math. Phys.* **12**, 157 (1971).
- [21] C. Chakraborty, P. Majumdar, *Class. Quant. Grav.* **31**, 075006 (2014).
- [22] S. Ashtekar and A. Sen, *J. Math. Phys.* **23**, 2168 (1982).
- [23] M. Mueller and M. J. Perry, *Class. Quant. Grav.* **3**, 65 (1986).
- [24] G. Holzegel, *Class. Quant. Grav.* **23**, 3951 (2006).
- [25] D. Bini, C. Cherubini, M. Mattia and R. T. Jantzen, *Gen. Relativ. Grav.* **35**, 2249 (2003).
- [26] S. Chandrasekhar, *The Mathematical Theory of Black Holes*, Clarendon Press, Oxford (1983).
- [27] P. Pradhan, *Class. Quant. Grav.* **32**, 165001 (2015).
- [28] C. W. Misner, *J. Math. Phys.* **4**, 924 (1963).
- [29] J. G. Miller *J. Math. Phys.* **14**, 486 (1973).
- [30] C. W. Misner, K. S. Thorn, J. A. Wheeler, *Gavitation* , W. H. Freeman (1973).
- [31] P. Pradhan, *JETP* **122** ,113 (2016).
- [32] M. Bañados, J. Silk, and S. M. West, *Phys. Rev. Lett.* **103**, 111102 (2009).
- [33] P. Pradhan, *Inter. J. Mod. Phys. D* **24**, 155086 (2015).
- [34] B. Mashhoon, *Phys. Rev. D* **31**, 290 (1985).
- [35] V. Cardoso et al., *Phys. Rev. D* **79**, 064016 (2009).
- [36] R. A. Konoplya, *Rev. Mod. Phys.* **83**, 793 (2011).
- [37] P. Pradhan, *Pramana-J. Physics*, DOI:10.1007/s12043-016-1214-x (2016).